AD-A065 470 AIR FORCE INST OF TECH WRIGHT-PATTERSON AFB OHIO F/G 4/2
DEVELOPMENT OF DOPPLER RADAR TECHNIQUES FOR SEVERE THUNDERSTORM--ETC(U)
1978 J D BONEWITZ
UNCLASSIFIED AFIT-CI-79-73 NL

1 OF 1
AD
A065470

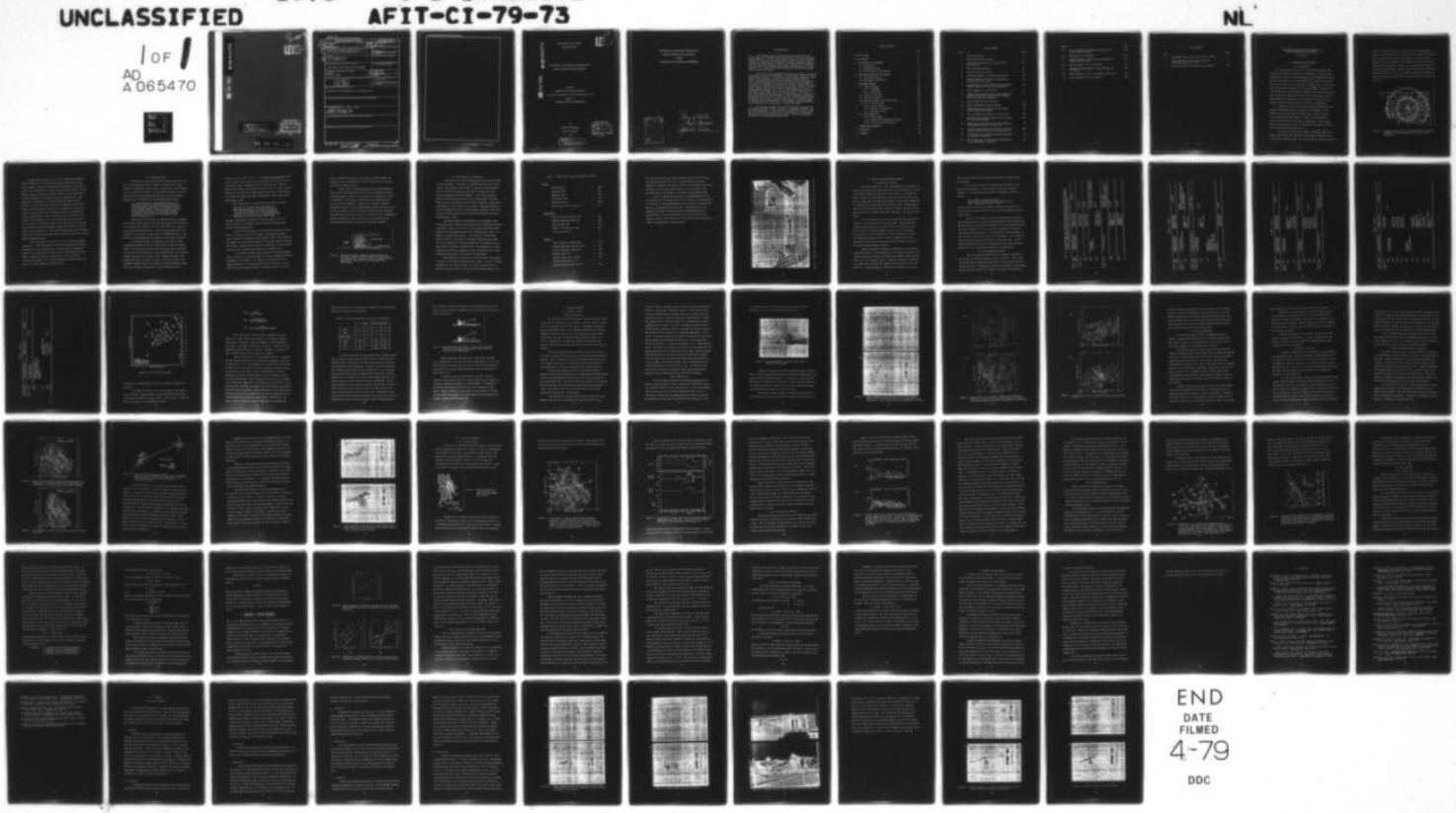

END
DATE
FILMED
4-79
DDC

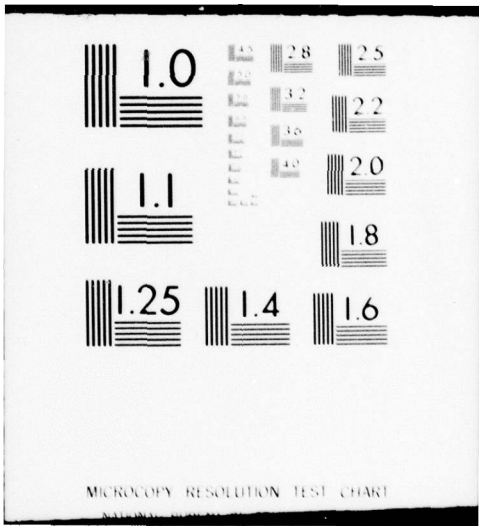
1.0
1.1
1.25
1.4
1.6
1.8
2.0
2.2
2.5
2.8
3.2
3.6
4.0
MICROCOPY RESOLUTION TEST CHART

UNCLASSIFIED

SECURITY CLASSIFICATION OF THIS PAGE (When Data Entered)

(14) AFIT-CI-79-73

REPORT DOCUMENTATION PAGE

READ INSTRUCTIONS BEFORE COMPLETING FORM

1. REPORT NUMBER: AFIT-CI-79-73
2. GOVT ACCESSION NO.
3. RECIPIENT'S CATALOG NUMBER

(6) 4. TITLE (and Subtitle): Development of Doppler Radar Techniques for Severe Thunderstorm Wind Advisories

5. TYPE OF REPORT & PERIOD COVERED: (9) Master's Thesis

6. PERFORMING ORG. REPORT NUMBER

(10) 7. AUTHOR(s): Joel David Bonewitz

8. CONTRACT OR GRANT NUMBER(s)

9. PERFORMING ORGANIZATION NAME AND ADDRESS: AFIT student at the University of Oklahoma

10. PROGRAM ELEMENT, PROJECT, TASK AREA & WORK UNIT NUMBERS

11. CONTROLLING OFFICE NAME AND ADDRESS: AFIT/CI, WPAFB OH 45433

(11) 12. REPORT DATE: 1978

13. NUMBER OF PAGES: 69

14. MONITORING AGENCY NAME & ADDRESS (if different from Controlling Office): (12) 78p.

15. SECURITY CLASS. (of this report): Unclassified

15a. DECLASSIFICATION/DOWNGRADING SCHEDULE

16. DISTRIBUTION STATEMENT (of this Report)

Approved for Public Release, Distribution Unlimited

17. DISTRIBUTION STATEMENT (of the abstract entered in Block 20, if different from Report)

18. SUPPLEMENTARY NOTES

FEB 8 1979

JOSEPH P. HIPPS, Major, USAF
Director of Information, AFIT

19. KEY WORDS (Continue on reverse side if necessary and identify by block number)

20. ABSTRACT (Continue on reverse side if necessary and identify by block number)

DD FORM 1 JAN 73 1473 EDITION OF 1 NOV 65 IS OBSOLETE

Ø12 20Ø

UNCALSSIFIED

SECURITY CLASSIFICATION OF THIS PAGE (When Data Entered)

THE UNIVERSITY OF OKLAHOMA

GRADUATE COLLEGE

DEVELOPMENT OF DOPPLER RADAR TECHNIQUES FOR SEVERE THUNDERSTORM WIND ADVISORIES

A THESIS

SUBMITTED TO THE GRADUATE FACULTY

in partial fulfillment of the requirements for the

degree of

MASTER OF SCIENCE IN METEOROLOGY

By

JOEL DAVID BONEWITZ

Norman, Oklahoma

1978

DEVELOPMENT OF DOPPLER RADAR TECHNIQUES FOR

SEVERE THUNDERSTORM WIND ADVISORIES

A THESIS

APPROVED FOR THE DEPARTMENT OF METEOROLOGY

By

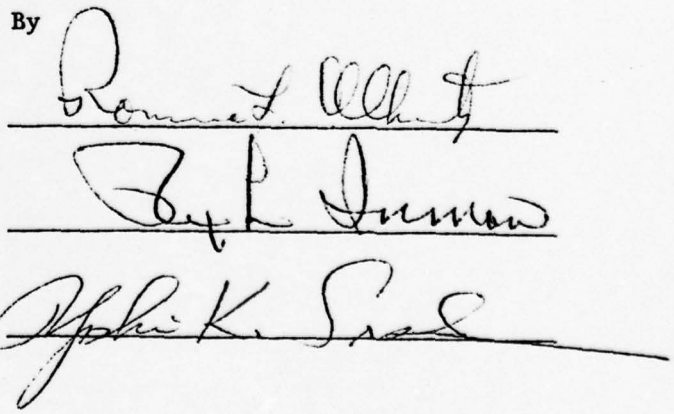

ACKNOWLEDGMENTS

This research was done while serving as the Air Force team member with the Joint Doppler Operational Project at the National Severe Storms Laboratory. My role in this program would not have been possible without the assistance and cooperation of Air Force Institute of Technology (Capt. Harry Hughes), University of Oklahoma Meteorology Department (Dr. Rex Inman), National Severe Storms Laboratory (Dr. Ed Kessler and Ken Wilk), and Air Weather Service (Capt. Ray Bonesteele). It was a pleasure to be a member of the JDOP experimental team with Don Burgess (NSSL) and Don Devore (NWS).

Much credit for my successful completion of this dual obligation program goes to my advisory committee, Drs. Ron Alberty (NSSL), Rex Inman, and Yoshi Sasaki (OU). I am grateful for their advice, assistance, and support in my commitment to both class studies and JDOP research. Capt. Ray Bonesteele deserves special recognition for his encouragement and assistance throughout this program. In many ways Ray was both a driving and a stabilizing force in the JDOP program. Rodger Brown (NSSL) and Don Burgess both gave unstintingly of their time to answer my questions. Much of this paper grew out of my discussions with these two outstanding individuals. All of these people reviewed this work one or more times during various phases of its development. I also thank Mike Kraus (AFGL) for his review and valuable suggestions; Leroy Fortner, Mike Weible, and Chuck Safford (NSSL) for their programming assistance; and Don Devore (pictured on the left in Figure 3) for gathering data at OKC WSFO for use in this research. Acknowledgment is gratefully given to Jennifer Moore and Chuck Clark for both graphics and photographics, and Evelyn Horwitz for assisting me in typing this paper.

Having spent the last 19 months in the Master's program at OU and working with NSSL on JDOP, I have had the opportunity to meet a lot of interesting people. I find that there are many more people to thank for their assistance and support than is possible here. I hope that I have been able to personally express how much I have enjoyed meeting, working with, and learning from each of you.

TABLE OF CONTENTS

	Page
LIST OF FIGURES	v
LIST OF TABLES	vii
1. INTRODUCTION AND BACKGROUND	1
1.1 Introduction	1
1.2 Thunderstorm Winds	4
1.3 JDOP Equipment and Procedures	7
2. REAL-TIME OBSERVATIONS AND RESULTS	11
2.1 Operational Summary	11
2.2 Wind Advisory Comparisons	12
3. SIGNATURE RESEARCH	22
3.1 Computer Program	22
3.1.1 Development	22
3.1.2 Truth check	23
3.2 Problems Encountered	28
3.3 Parameter Composites	29
3.4 Radar Azimuth/Wind Direction Geometry	30
3.5 Gust Front Examination	35
3.5.1 General features	35
3.5.2 Vertical cross-section	38
3.5.3 Downdraft source	41
3.6 Data Comparisons	44
3.6.1 Timing study	44
3.6.2 Surface versus Doppler wind study	49
3.6.3 Future technique improvement	52
4. SUMMARY AND CONCLUSIONS	54
5. REFERENCES	57
6. APPENDIX	60

LIST OF FIGURES

Figure		Page
1	JDOP operating area	2
2	Thunderstorm outflow schematic	6
3	Operational configuration of multimoment and color displays	10
4	NSSL 1977 surface network	18
5	Elevation angle error effect	21
6	Tornado photograph at 1430 CST on 20 May 1977	24
7	Doppler displays of velocity and reflectivity for 20 May 1977 (1412 CST)	25
8	Cross-section of Doppler reflectivity and radial velocity contours at 1414 CST on 20 May 1977	26
9	Same as Figure 8, but at 1430 CST	27
10	Doppler radial velocity contour cross-section for 3 May 1977 (2125 CST) showing areas of maximum reflectivity and spectrum width	31
11	Same as Figure 10, but at 2127 CST	31
12	Radar azimuth/wind direction geometry	32
13	Doppler displays of velocity and reflectivity for 28 June 1977 (1727 CST)	34
14	PPI time sequence of squall line on 3 May 1977	35
15	Cross-section of Doppler radial velocity contours on 3 May 1977 (2125 CST)	36
16	Analog plot of surface strip chart for Newcastle (NCL) mesonetwork site for 3 May 1977	37
17	Vertical cross-section at 2127 CST on 3 May 1977 showing Doppler reflectivity and radial velocity	39
18	Surface plot of θ_e computed from mesonetwork data on 3 May 1977 (2125 CST)	42
19	Skew T-log p plot of sounding data from Oklahoma City at 1800 CST on 3 May 1977	43

Figure		Page
20	Scatter diagram of timing data from gust front on 3 May 1977 (2125 CST)	48
21	Regression line explaination	48
A-1	Doppler displays of velocity and reflectivity for 30 May 1977 (2014 CST)	64
A-2	Same as Figure A-1, but at 2058 CST	65
A-3	Straight line wind damage at Lawton, Oklahoma on 30 May 1977	66
A-4	Same as Figure A-1, but at 1620 CST on 28 June 1977	68
A-5	Same as Figure A-4, but at 1700 CST	69

LIST OF TABLES

Table		Page
1	NSSL Norman Doppler radar characteristics (1977).	8
2	Wind advisories and severe wind occurrences during JDOP operations in 1977.	13
3	W2 wind advisory skill statistics from JDOP 1977.	20

DEVELOPMENT OF DOPPLER RADAR TECHNIQUES FOR SEVERE THUNDERSTORM WIND ADVISORIES

J. D. Boneritz

1. INTRODUCTION AND BACKGROUND

1.1 Introduction

It is generally accepted that a well-calibrated weather radar can measure the relative strength of thunderstorms. The current operational network radars, the National Weather Service (NWS) WSR-57 and the Air Force Air Weather Service (AWS) FPS-77, only measure reflectivity. Even in rare cases when a very intense circulation results in the "hook" echo, the associated tornado may have already formed. Likewise, the classic "thin line" echo frequently indicates a gust front, but does not give a quantitative measure of the associated wind strength. Both of these reflectivity characteristics are limited to a relatively short detection range and are seen only in the best of circumstances.

The Doppler weather radar measures radial displacement of the scatters (hydrometeors) and thus provides wind information. The National Severe Storms Laboratory (NSSL) began in 1970 to develop a 10 cm pulsed Doppler radar system to advance the understanding of internal flow patterns in large severe thunderstorms. Lemon et al. (1977) provide a good overview of the application of Doppler radar to severe storm detection and warning.

The success of researchers at NSSL and elsewhere (Smith and Holmes, 1961; Atlas, 1963; Lhermitte, 1964; Burgess, 1976) has led to consideration of Doppler radar as the next generation operational system.

However, excellent results in a research mode do not automatically establish that the same would be possible in an operational environment. The Joint Doppler Operational Project (JDOP) was designed to test Doppler radar in an operational mode (Johannessen and Kessler, 1976). Using the NSSL Norman Doppler radar, an experimental team composed of forecasters from NWS, AWS, and NSSL issued severe weather advisories to NWS offices and AWS sites within a 230 km operating radius (Figure 1) during the Springs of 1977 and 1978. This report deals only with the 1977 data.

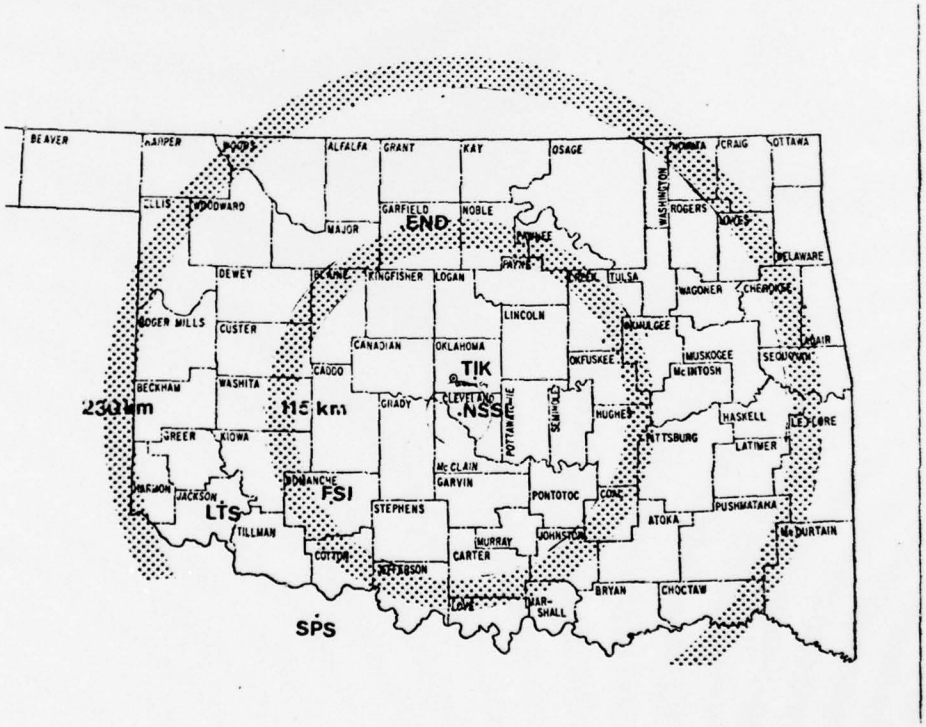

Figure 1. Regions of ground clutter (shaded) unusable for velocity estimation. Military bases marked by three letter identifiers.

Through research efforts at the Air Force Geophysics Laboratory (AFGL) and NSSL (e.g., Donaldson, 1970; Burgess, 1976; Brown et al., 1978) signatures have been identified for the mesocyclone and tornadic vortex. These signatures are radial wind patterns that appear as closed velocity couplets since zero velocity is detected along a radial from the radar through the circulation center (flow perpendicular to the radar beam). Signatures can be distinguished from numerous other regions of cyclonic shear in the storm by the amount of shear and the presence of time and height continuity in the signature. Intensity of the shear and horizontal scale distinguish between a mesocyclone and tornado vortex signature. While the Air Force was interested in the testing of these signatures in an operational mode, there was equal or greater interest in the effectiveness of the Doppler radar in detecting and advising on potentially damaging straight line winds of convective origin. While tornadoes are a rare event threatening Air Force resources, the much more frequent strong thunderstorm cold air outflow winds contain extensive damage potential.

As stated by NSSL Staff (1971), the "forecasting of hazardous wind gusts is a four-fold problem of detection, interpretation, pattern extrapolation of the smoothed field, and prediction of maximum gusts." Goals of this research were to gather wind data while participating in JDOP, to issue wind advisories in real time, to test the initial successes and failures, and to begin development of Doppler radar techniques for severe thunderstorm wind advisories.

1.2 Thunderstorm Winds

While there has been much research on thunderstorms since the time of the Thunderstorm Project (Byers and Braham, 1949), recent studies of thunderstorm outflow (Charba, 1972; Walters, 1975) indicate needs for additional knowledge. With the advent of Doppler radar as a research tool for studying thunderstorm winds, there is increased possibility of meeting research needs stated by Charba (1972):

> ...a need remains for a complete definition of the structure of kinematic and thermodynamic variables in three dimensions. Furthermore, for improved forecasting of the gust front, it will be necessary to obtain a better understanding of the mechanism of formation and maintence of the gusty air mass and to clarify the mechanics of its horizontal propagation outward from the parent storm.

Most Doppler radar studies of thunderstorms (e.g., Armstrong and Donaldson, 1969; Burgess, 1976; and Brown et al., 1978) and thunderstorm outflow (e.g., Brandes, 1975, 1976, 1977) have been associated with a well-developed mesocyclone. The mesocyclone signature is now accepted as a precursor of severe weather, including high winds. Questions about the non-mesocyclone related gust front remain unanswered.

A starting point is the examination of the nature of the thunderstorm outflow, termed the "cold-air dome" by Byers and Braham (1949). While a portion of this outflow has become known as the gust front due to the resulting surface wind changes (Colmer, 1971) and wind changes "coincident with a pressure surge" (Charba and Sasaki, 1971; Charba, 1972, 1974), the gust front may be usefully defined as "the convergent boundary between storm outflow and inflow" (Brandes, 1976); that is, the "boundary separating the cold air outflow from the

displaced warm air" (Goff, 1976). In the Glossary of Meteorology (1970) the gust front is known only as the "first gust". This cold outflow air mass has been shown to propagate out from the parent cell (Byers and Braham, 1949; Colmer, 1971; Charba, 1974; Goff, 1976). It has also been shown that a wind direction change normally occurs prior to the arrival of the gust front (Byers and Braham, 1949; Colmer, 1971; Charba, 1974; Greene et al., 1977).

Goff (1976) makes a very valid observation when he states:

> Each outflow is affected by the behavior and character of the parent thunderstorm and by the flow and stratification in both the warm ambient air and the cold outflow air. This produces much variation from case to case and makes difficult the description of a representative outflow model.

Likewise, meteorological parameters measured at surface sites are greatly affected by atmospheric conditions, most notably low-level stability (Greene et al.,1977).

Colmer (1971) and Charba (1972) found good correlation between speed of the parent echo and wind damage. Wind damage increased in direct proportion to the speed of echo movement. Goff (1976) found that the maximum winds were directly related to propagation speed of the gust front itself. Walters (1975) related the maximum gusts to the pressure gradient across a pressure dome created by the downdraft air.

It is generally assumed that one aspect of the downdraft/gust front interaction is vertical transport of horizontal momentum from mid-troposphere to the surface. Goff (1976) sees this conservation of higher momentum air in the outflow ahead of the parent cell. Walters (1975) shows apparent conservation of horizontal velocity "with some

loss to turbulent dissipation" and a change in wind direction. He presents a case for adding 90° to the lower mid-level wind direction to predict the gust direction.

Several models of thunderstorm outflow have been developed. Charba (1972, 1974) approached the gust front as a gravity wave with very good success. However, he also states that "the precise role of the downdraft in the formation and maintenance of thunderstorm gust fronts is still problematic." Figure 2 is a schematic diagram of thunderstorm cold air outflow showing multiple surges and both the warm and dry air inflows. While few numerical models have been developed that concentrate on the gust front, one of the most recent, developed by Mitchell and Hovermale (1977), seems to provide good results and promises continued advances in gust front numerical modeling.

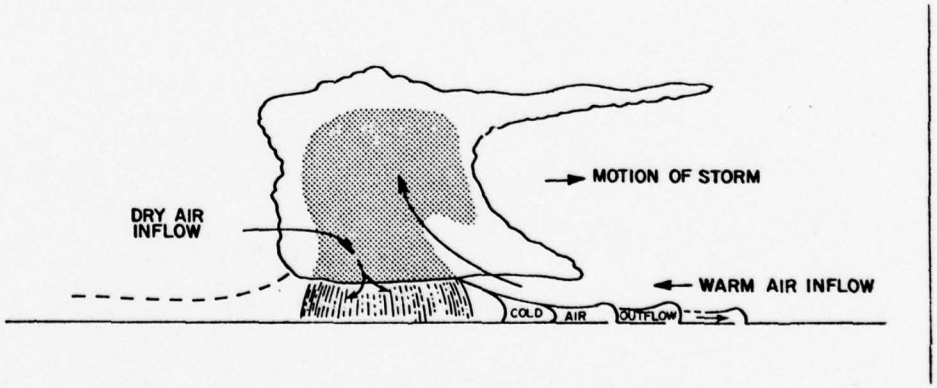

Figure 2. Thunderstorm outflow schematic showing multiple cold air surges. Region of strong radar reflectivity due to high precipitation content is stippled. Outflow into the thunderstorm's wake exists below the dashed line. (Goff, 1976)

1.3 JDOP Equipment and Procedures

JDOP operated from NSSL's Norman Doppler radar facility (NRO) in Norman, Oklahoma. This radar is a modified FPS-18 with 10 cm wavelength. Radar characteristics (Table 1) include a narrow beamwidth, accurate reflectivity estimates, and real-time processing of mean velocity and spectral width information. A dual pulse repetition frequency (PRF) processing system allows intensity data to be taken during a long pulse repetition period (460 km range) and velocity data interspersed in a short period (115 km range). Velocity estimates are correctly positioned in space by making comparisons between the reflectivity and velocity samples, thus filtering out multiple trip echoes (Burgess et al., 1978).

The Norman Doppler was interfaced to a Ling computer which processed the data (removing range ambiguities and performing coordinate conversion). These data were fed to a Vector General graphics system displaying the Multimoment Display (MMD) (Burgess et al., 1976), and a Computer Automation (CA) computer. The CA computer presented the Doppler data on a color display, described by Burgess et al. (1978). This color display used 15 velocity categories with maximum color contrast between velocities of opposite sign. The combination of colors displaying reflectivity emphasized the higher intensities (from bright color/high reflectivity to dull color/low reflectivity).

JDOP operated in a continuous surveillance mode which provided all data in a PPI (Plan Position Indicator) format. In order to obtain information at more than one height in a storm, the radar antenna control was programed with a series of elevation angle changes. Thus,

Table 1. Norman Doppler radar characteristics (1977).

General		
Wavelength (cm)	=	10.52
Peak power (kW)	=	750
Beamwidth (deg.)	=	0.81
Pulse length (m)	=	150
Antenna gain (dB)	=	46.8
Antenna rotation rate (deg. s^{-1})	=	6.0
Reflectivity		
Pulse repetition frequency (Hz)	=	325
Maximum unambiguous range (km)	=	460
Range increment (m)	=	600
Number of data bins per radial	=	762
Intensity resolution	=	1.3
Velocity		
Pulse repetition frequency (Hz)	=	1300
Maximum unambiguous velocity (m s^{-1})	=	±34
Maximum unambiguous range (km)	=	115
Range increment (m)	=	150
Number of data bins per radial	=	762
Velocity resolution (m s^{-1})	=	1
Spectral width resolution (m s^{-1})	=	0.5

the storm was viewed at the lowest elevation angle on the first scan, and each subsequent PPI scan was at a higher elevation until the sequence was completed, the antenna lowered, and the sequence restarted. The four to six elevation angles used in this "tilt sequence" were determined by the distribution of the storms in the operating area.

The two displays (MMD and color) were placed together in the operations area of the Norman Doppler control room to aid in interpretation (Figure 3). When predetermined criteria were met, an advisory was phoned to the appropriate warning office. Mesocyclone criteria as developed by Donaldson (1970) and modified for operational use by Burgess (1976) were well defined prior to the start of JDOP, but no criteria existed for wind advisories. This research reflects the first attempt at development of a wind signature.

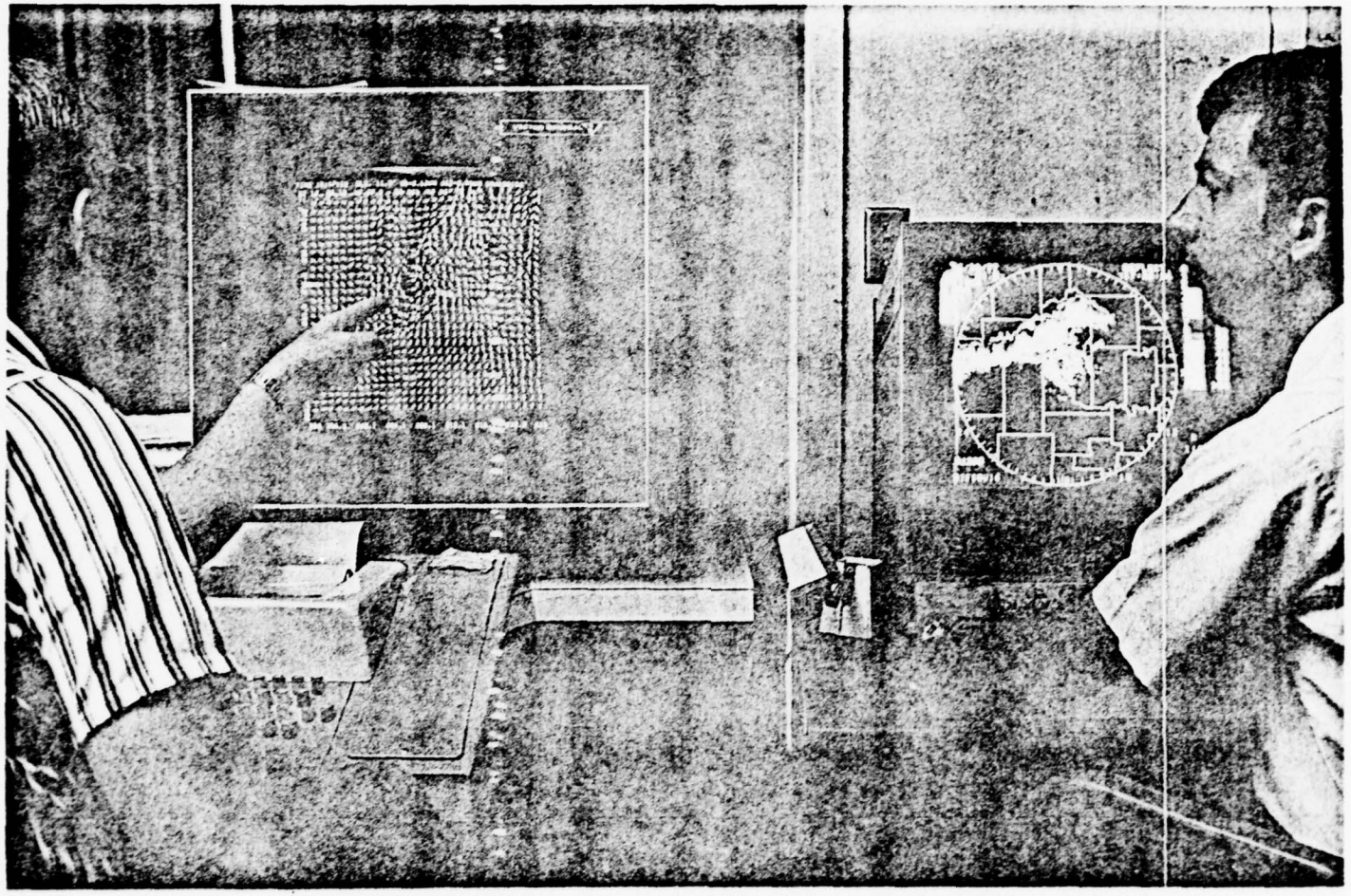

Figure 3. Operational configuration of the multimoment display (left) and the color display (right).

2. REAL-TIME OBSERVATIONS AND RESULTS

2.1 Operational Summary

During JDOP operations in 1977, the experimental team spent 175 hours at the radar site, issued 45 advisories, and recorded over 41 hours of PPI data on digital tape for use in post-analysis. An attempt was made to follow the initial plan which called for a tilt sequence to be placed on tape every 20 minutes while JDOP was "in operation", defined as the JDOP team having operational control of the radar. Requirements to share the radar with NSSL research operations caused occasional loss of radar control for extended time periods, frequently at the most critical times.

Of the 45 advisories, 11 were for events meeting wind advisory criteria. Two categories were used during JDOP. A W2 advisory was issued for winds greater than or equal to 25 m s^{-1} ($\approx$50 knots), and a W1 advisory was issued for winds less than 25 m s^{-1}, but greater than or equal to 18 m s^{-1} ($\approx$35 knots). These categories were based on existing AWS warning criteria. Since no "signature" had been discovered, advisories were based on the radial component of wind for the lowest elevation angle being used.

Eight W2 advisories and three W1 advisories were issued while JDOP was operating. Advisory updates were not counted separately if the original advisory was issued while JDOP had operational control of the radar (i.e., "in operation" time). In general, advisories to military sites (AWS) were for events that appeared likely to affect their location (i.e., "point warnings"), and advisories to NWS were for events

within the JDOP operating area without establishing a single verification location.

All of the wind cases for JDOP during the operations in 1977 appeared on eight days. A general summary of each day is given in Appendix A. In examining advisory success, terminology is used as follows:

Hit = Forecast event which occurs
False Alarm = Forecast event which does not occur
Miss = Unforecast event which occurs

In this study, the event is the convective outflow meeting W1 or W2 advisory criteria, and the forecast is the advisory issued by the experimental team.

Table 2 is a comprehensive list of wind advisories and actual severe wind occurrences. Actual wind occurrence data were obtained from NWS Storm Data (U.S. Department of Commerce, 1977), the NSSL Mesonetwork (as shown in Figure 4, an array of remote data recording sites), and reporting station observations. For verification of wind advisories to NWS, an actual wind occurrence must have been located in the vicinity of the storm within one and a half hours of the advisory time. For the military advisories actual wind occurrence within this time period and within 9 km of the site warned was required for verification.

2.2 Wind Advisory Comparisons

Once the real-time advisory portion of JDOP was concluded, it was necessary to examine successes, failures, and skill. Since it had been assumed that the advisories were likely to be for events that were already occurring, no lead-time statistics were obtained in post-analysis. However, from the digital data recorded in real-time, the advisories,

Table 2. Wind advisories and severe wind occurrences during JDOP operations in 1977. (Range and azimuths given with respect to Norman Doppler. Three letter identifiers refer to NSSL mesonetwork sites.)

DATE	TIME (CST)	ADVISORY/LOCATION (AZRAN from NRC)	EVENT/LOCATION (AZRAN from NRO)	REMARKS
3 May	1815		27 ms^{-1}/Altus (250°/177 km)	W2 MISS
	1833		29 ms^{-1}/Tipton (240°/176 km)	W2 MISS
	2139	W2 Update (250°/20 km)		2047 CST--not full operational Initially issued at 250°/70 km
	2245		Damage in OKC 2 roofs blown off windows broken	W2 HIT
14 May	1746	W2 (279°/210 km)		W2 FALSE ALARM 15 ms^{-1} winds at 1757 CST in NSSL subsynoptic network
	1930		Damaging wind/ Taloga (305°/160 km)	W2 MISS
	2200		Damaging wind/ Anadarko (260°/67 km)	W2 MISS

Table 2. (cont.)

DATE	TIME (CST)	ADVISORY/LOCATION (AZRAN from NRO)	EVENT/LOCATION (AZRAN from NRO)	REMARKS
14 May (cont.)	2244	W2 (229°/80 km) 15 km WSW Rush Springs		W2 HIT (OKC WSR-57 overlays show same storm responsible for both event and advisory)
	2325		Damaging wind/ Marlow (215°/80 km)	
15 May	2129	W1 (approaching OKC)		W1 FALSE ALARM
16 May	1900	W2 (285°/200 km) 9 km N Cheyenne		
	1920		High wind/ Leedy (293°/194 km)	W2 HIT
	1943	W2 Update (288°/160 km to 296°/170 km) 9 km E of line from Butler to 28 km NE of Leedy		
19 May	1230		27 ms^{-1}/Hobart (262°/150 km)	W2 MISS

Table 2. (cont.)

DATE	TIME (CST)	ADVISORY/LOCATION (AZRAN from NRO)	EVENT/LOCATION (AZRAN from NRO)	REMARKS
19 May (cont.)	2037	W2 (158°/110 km) 9 km N Gene Autry		
	2045		Damaging wind/ Overbrook (167°/130 km)	W2 HIT
	2110		26 ms^{-1}/Ardmore (165°/120 km)	
20 May	2205	W2 (050/42 km) 4 km N McLoud		W2 FALSE ALARM
	2310		30 ms^{-1}/ELR (304°/56 km)	
	2316		29 ms^{-1}/EMC (175°/65 km)	W2 MISS
	2320		31 ms^{-1}/GLD (190°/13.4 km)	
30 May	1830	W1 (010°-020°/45 km)		W1 HIT to OKC FALSE ALARM to Tinker AFB

Table 2. (cont.)

DATE	TIME	ADVISORY/LOCATION	EVENT/LOCATION	REMARKS
30 May (cont.)	2010		29 ms^{-1}/DUT (267°/58 km)	
	2016	W2 (271°/42 km) 15 km SW Tuttle		W2 HIT
	2025		26 ms^{-1}/VNW (258°/64 km)	
	2028		27 ms^{-1}/PSW (262°/50 km)	
	2100		29 ms^{-1}/VSW (252°/69 km)	
	2106	W2 Update (260°/72 km) 6 km NE Anadarko		
	2110		30 ms^{-1}/VRD (253°/58 km)	
	2125		Damaging wind/ Anadarko (255.3°/74.1 km)	
	2128		32 ms^{-1}/CNW (247°/77 km)	
	2206		Major wind damage/ Lawton (231°/110 km)	

Table 2. (cont.)

DATE	TIME	ADVISORY/LOCATION	EVENT/LOCATION	REMARKS
28 Jun	1631	W1 (320°/73 km) 19 km NE Okarche		W1 HIT
	1643	Update and Upgrade W2 (320°-340°/45-50 km) 15 km N Yukon to 9 km W Edmond		
	1705		25 ms^{-1}/KTVY Tower (356°/37 km)	
	1730		26 ms^{-1}/NE OKC	W2 HIT
	1736		21 ms^{-1}/OKC	

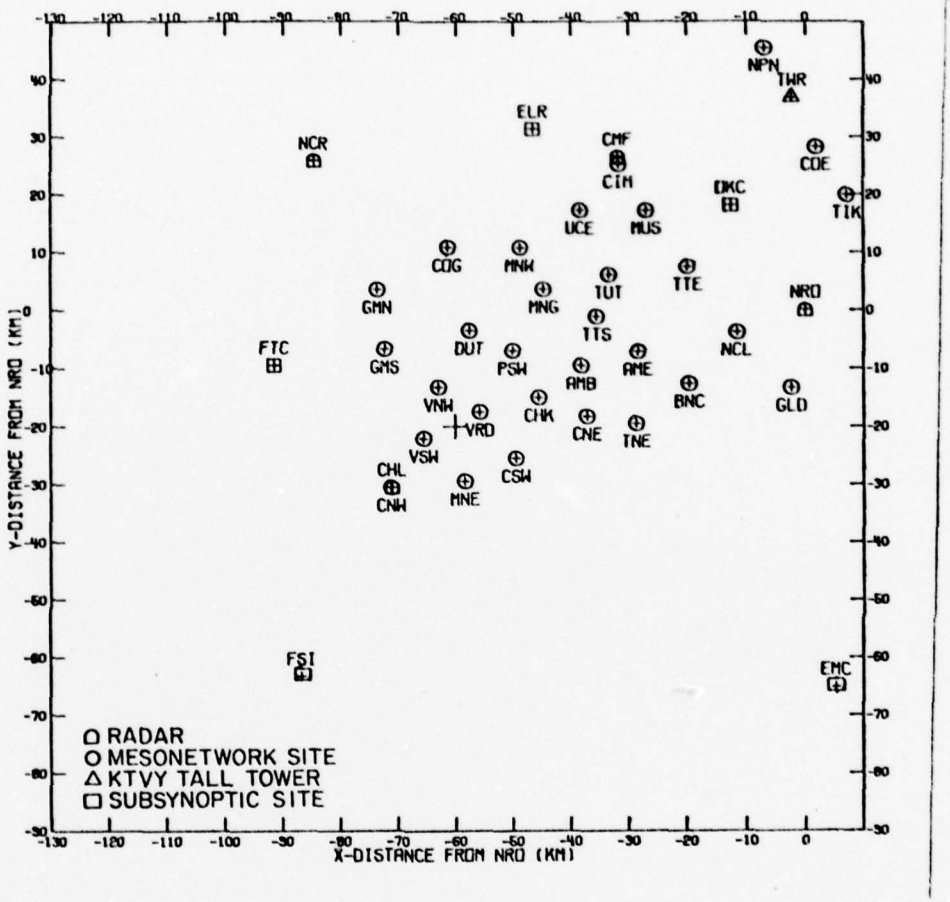

Figure 4. NSSL 1977 surface network.

and surface data available after the fact, a measure of success was obtained.

The objective evaluation, the Critical Success Index (CSI), gives credit for a high probability of detection (POD) and low false alarm rate (FAR) (Donaldson et al., 1975). A CSI of 1.0 is perfect and 0.0 is no success. It is calculated as follows:

$$POD = \frac{Hits}{Hits + Misses}$$

$$FAR = \frac{False\ Alarms}{Hits + False\ Alarms}$$

$$CSI = \frac{Hits}{Hits + Misses + False\ Alarms}$$

Due to the nature of the W1 advisory (relatively low wind speed), it is quite possible that damage, if any occurred, might go undetected or unreported. Since wind damage is a key to obtaining verification, the number of W1 Misses is not known. Likewise, the one False Alarm could be subject to question. Therefore, no attempt was made to develop a CSI from the two W1 Hits recorded.

Table 3 is the result of the W2 advisory efforts. An attempt was made during post-analysis to determine what conditions resulted in an advisory Miss. It is quite apparent that a Miss could be due either to the failure of the operator to properly interpret the radar data or to the failure of the radar to detect the high winds. As stated previously, the lowest elevation angle in the tilt sequence was used for high wind detection. While the general concept was one of looking at low level winds, there was no firm definition of "low level". It was recognized that the higher one looked in the storm the less correlation would exist with the surface. During post-analysis it was found that an improved success rate was achieved when the data were obtained from an elevation angle that centered the radar beam at or below 1 km. In effect, this 1 km limitation placed a range limit at the end of the

first trip (115 km). The statistics are divided into first and second trip data to reflect this range effect.

Table 3. W2 wind advisory skill statistics from JDOP 1977.

	1st TRIP		2nd TRIP	TOTAL
		α		
HIT	4	1	1	6
MISS	1	2	3	6
FALSE ALARM	0	1	1	2
POD	80%		25%	50%
FAR	0%		50%	25%
CSI	80%		20%	43%

It was also discovered in post-analysis that a problem existed with the radar elevation angle that affected both real-time and post-analysis studies. Elevation errors found during quality control were not corrected by antenna adjustments. Instead, correction values were made available for application to the digitial data. As the computer programs used raw data tapes and applied these corrections, it became apparent that on a number of days the elevation angle believed to be in use and what was actually being seen differed considerably. The two possible effects of this elevation angle error (α) are shown in Figure 5. Since the lowest elevation angle was used, the radar may have been looking into the ground or above the 1 km layer. Consequently, those cases with elevation corrections resulting in no data between 0 and 1 km were separated in the statistics as another cause of advisory misses.

The CSI (Table 3) would have slipped to 56 percent had data with elevation errors been included. Combining first and second trip data yields a CSI of 50 percent.

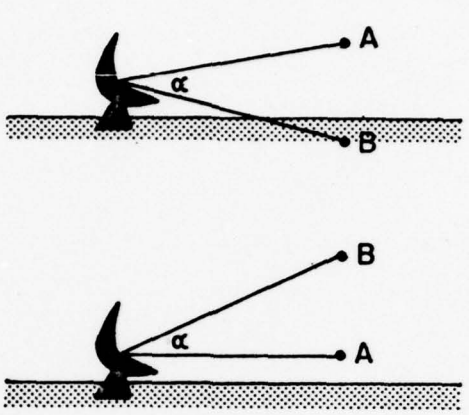

Figure 5. Elevation angle error effect. Point A is the apparent position of a return due to elevation angle error (α). Point B is the actual target.

These same effects (operator error, radar error, elevation error, range) could be the cause of advisory False Alarms. In fact, the two W2 False Alarms appear to be the result of range (210 km placed the lowest data at 3.1 km) and negative elevation angle (a real-time 0.1° was in fact -0.7°).

It should also be pointed out that in one case a Hit was recorded in spite of the range and in another case a Hit was logged even though the antenna was actually at a -0.6° elevation. No definitive conclusions with respect to the CSI can be drawn from such a small sample. However, results do indicate that a certain amount of success can be expected with Doppler radar and a properly aligned antenna even without a sophisticated wind signature.

3. SIGNATURE RESEARCH

3.1 Computer Program

3.1.1 Development

In the normal research mode, digital radar data obtained at NSSL is not used for analysis in its raw format. Instead, a request is made for a certain batch of data to be "archived". The Computer Data Processing section (CDP) takes the data, applies calibration and correction (primarily azimuth, elevation, time, and timing) terms, and converts reflectivity, velocity, and spectrum width raw data into dBZ, m s^{-1}, and m s^{-1} respectively. In addition, anomalous and erroneous data points are removed when detected, and range and velocity folded data are unfolded.

Due to time limitations and the number of data tapes used in this study, analysis was done using raw data tapes and modified computer programs. Initial examination of the data fields was done from a printout of Doppler parameters in azimuth-range format produced from raw tapes (Raw B-Scan). Cases were then selected for further analysis.

The Raw B-Scan program written by Leroy Fortner (CDP) was merged with an analysis program written by Rodger Brown and Chuck Safford (both in the Meteorological Research Group). The resulting data were then interpolated onto a quasi-horizontal surface with 1 km grid spacing and smoothed using a one pass Cressman weighting function (Cressman, 1959). This smoothed data field was stored on disk file and then contoured for plotting by a second program.

Real-time data were acquired with range gate spacing of 150 m. However, only every third data point was processed giving a range

interval of 450 m. The final product was a 60 X 60 km quasi-horizontal grid with a North-South, East-West orientation. The Cressman filter used a horizontal radius of influence which was set depending on the actual data spacing. Since data spacing is range dependent, azimuthal data spacing could be computed using the 0.8^{o} beamwidth and azimuthal sampling interval (either 1^{o} or $1/2^{o}$). The greatest detail could be obtained using a horizontal radius of influence less than two times the data spacing, but this resulted in an extremely rough field. As this radius is increased, additional data points are averaged and the pattern becomes smoother. This smoothing was done only in the horizontal as data were restricted to a single cross-section (i.e., a single elevation angle). The center of the grid was located at the same height above the ground as the center of the radar beam at that range. Since the height difference across the 60 km grid is relatively minor with the small elevation angles used, the grid was assumed to be quasi-horizontal at the same height as the center position. Data were accepted into the analyzed pattern with as few as one data point. The number of data points used at every grid location was also printed out and used to identify possible problem areas due to insufficient sampling.

3.1.2 Truth check

Once the computer programs were merged and debugging was in process, it was necessary to find a suitable case such that the output data could be checked to verify program success. It was also desirable that this test case be of an easily identifiable event, such as a mesocyclone. During JDOP data gathering such an event took place on May 20th when a tornado struck Altus AFB, Oklahoma (Figure 6). This

case not only provided a check on program success, but also the opportunity to study a significant case during JDOP.

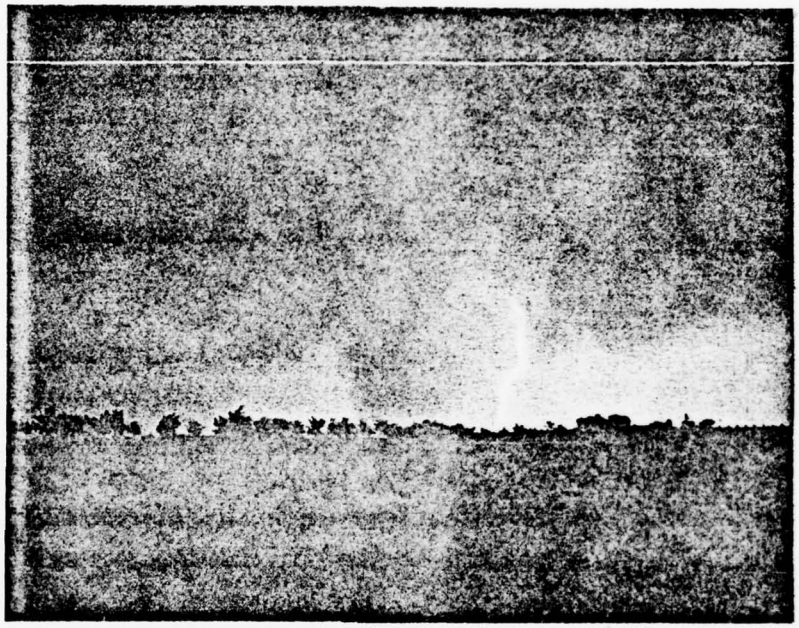

Figure 6. Tornado photograph (courtesy of Altus AFB) at 1430 CST on 20 May 1977.

Height and time continuity criteria (Burgess et al., 1978) were met at 1406 (all times given as Central Standard) for a mesocyclone 5 km south of Altus, Oklahoma (Figure 7). An advisory was passed to Altus AFB and to the Oklahoma City Weather Service Forecast Office (OKC WSFO). Altus AFB was hit by the tornado at 1430, causing considerable damage. The mesocyclone was tracked until just after 1500.

The computer program revealed an identifiable mesocyclone at the location where it was identified in real-time (Figure 8 and 9). To

(a)

(b)

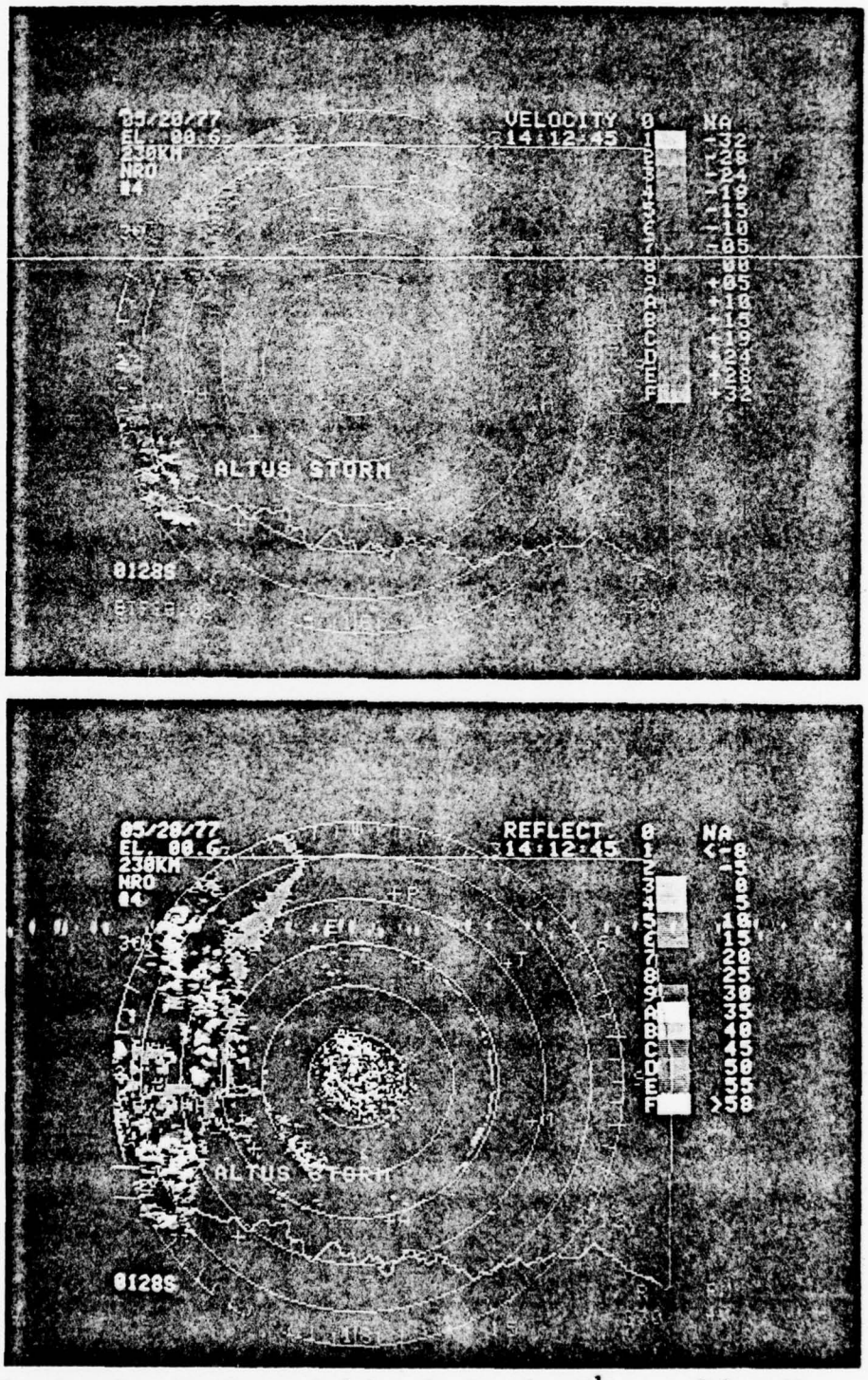

Figure 7. Doppler displays of (a) velocity (m s^{-1}) and (b) reflectivity (dBZ) for 20 May 1977 (1412 CST). Mesocyclone is at 246°/180 km. Scope range is 230 km and range marks are 40 km.

(a)

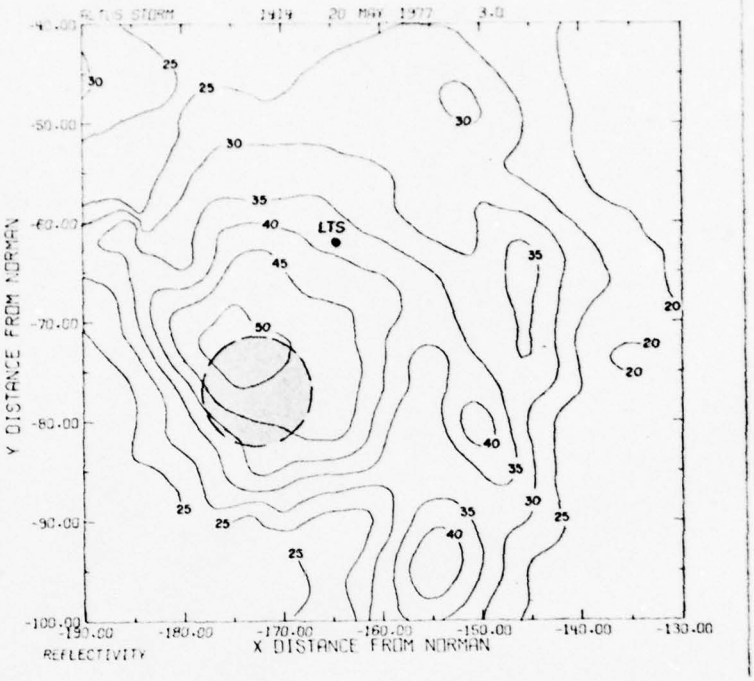

(b)

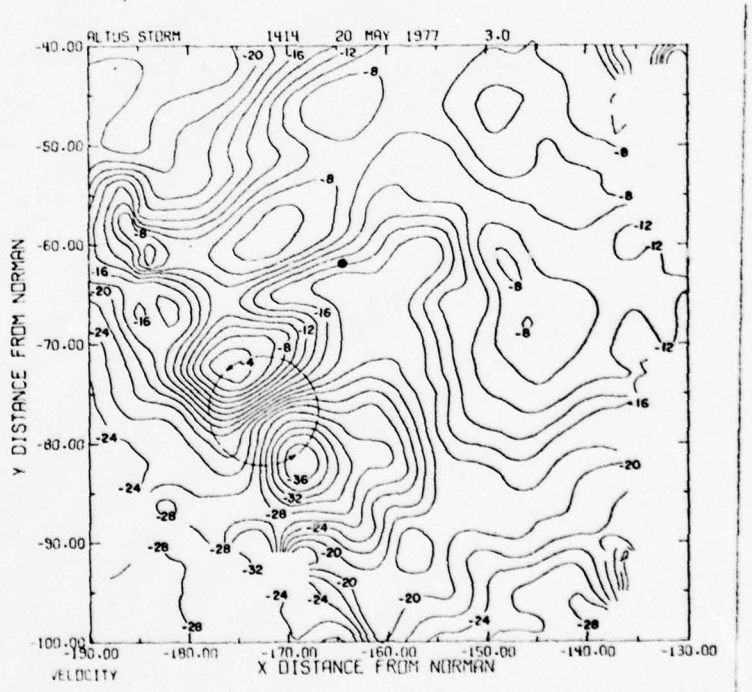

Figure 8. Cross-section at 3 km height of Doppler (a) reflectivity (dBZ) and (b) radial velocity (m s^{-1}) contours at 1414 CST on 20 May 1977 showing mesocyclone approaching Altus AFB (LTS).

(a)

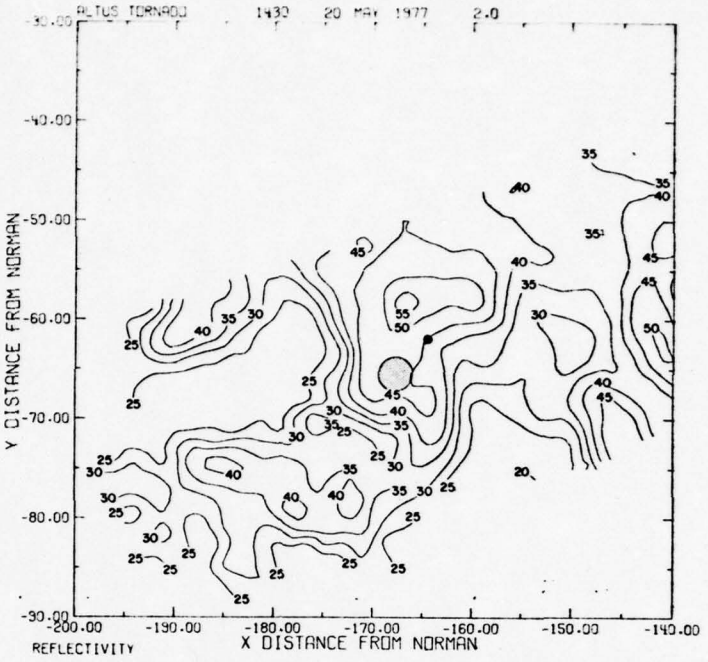

(b)

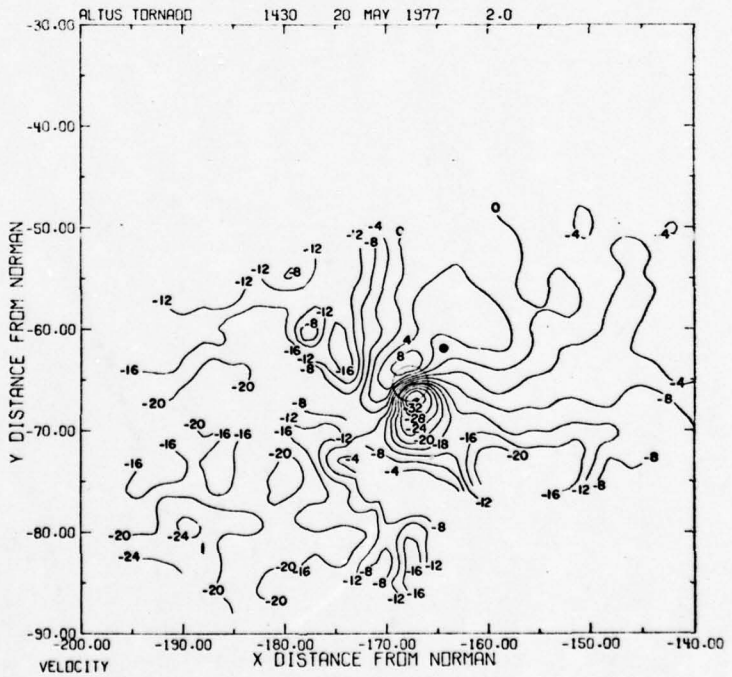

Figure 9. Same as Figure 8, but at 1430 CST and cross-section height is 2 km.

further check for discrepancies in the processed data, this contoured output was compared with integrator values recorded on the raw tape. Computer processing was verified by selected hand calculations. This was the primary check to insure that the velocity data was being positioned properly, and that signal-to-noise threshold and other checks were working properly to exclude bad data points.

3.2 Problems Encountered

As the analysis began, a number of problems became quite apparent. Some of these problems had been considered during the planning stages of JDOP, but the significance of others was not obvious until after completion of the operational test period.

The number of real-time cases available for study was rather limited. The improved success rate (higher CSI) for radar data obtained in the first kilometer above the surface implied that the correlation between that data and actual wind occurrences at the surface was stronger than for higher layers. Thus it was decided that the signature research in the study should concentrate on cases where data was available at or below 1 km. Limiting the study to these cases further reduced the size of the data set, and the elevation angle errors that caused questionable data to be used in real-time reduced the data set even further.

Another restriction on the data set was the fact that digital data were only recorded every 20 minutes. This meant that no time continuity analysis was possible. Much is yet unknown of thunderstorm life cycle and there is no objective way to predict whether cold air outflow is transitory or long lived for particular events. It is quite

possible that an event seen in real time escaped being recorded.

Unless there is major damage or a wind recording site in the correct location, strong winds are likely to escape verification. Verifcation is also complicated by the fact that the radar data are at some level above the surface. What will happen at the surface depends on variables such as terrain, low level stability, and actual height of the data above the ground.

Because storm motions were not used in real time advisories, there was no attempt to record them. Likewise, storm tops were not recorded. Both of these items might have provided additonal useful information, but are not available.

3.3 Parameter Composites

It would be prohibitive, even if desirable, to post-analyze all available digital data. Thus, it was decided to consider data closest to an advisory time or to the time of occurrence of a high wind event to determine what caused the advisory to be issued or why might an event have been missed. As in real time, only the lowest elevation angle data were used, and as discussed earlier the data to be examined were required to be at or below 1 km.

For each of these cases the digital data were processed and the contour fields of Doppler reflectivity (dBZ), radial velocity (m s^{-1}), and spectrum width (m s^{-1}) were studied. Using a light table, each set of contours was examined in composite form. Figure 10 is typical of the cases examined. The area of highest velocities falls outside the maximum reflectivity region. This should be expected at the lower levels since the strong outflow should be moving out away from the high

reflectivity core. Also, as seen from the composite, the high winds do not fall in a region of maximum spectrum width. The fact that it is not a maximum at this level should not be surprising as the outflow is relatively organized, and thus the scatter in the samples is not pronounced. However, outflow turbulence does exist as the outflow does not stand out from other portions of the cross-section as a spectrum width minimum.

It was thought that a different result might be seen in the mid-levels of the storm due to storm organization around the 4 to 6 km level. However, as can be seen in Figure 11, the 4.1 km cross-section of this same storm does not reveal an identifiable pattern.

3.4 Radar Azimuth/Wind Direction Geometry

As Doppler radar sees only the radial component of the wind, the orientation of the wind direction with respect to the radar beam is important. Winds perpendicular to the radar beam will register zero velocity as they have no component along the beam. Similarly, winds parallel to the beam will be registered in full. A logical improvement over issuing advisories based on the radial component would be some technique to convert from radial to true wind velocity. This can be done in a selected area through use of a multiple Doppler network, but the multiple Doppler approach is not feasible operationally.

As can be seen from Figure 12, simple trigonometric relationships allow computation of true horizontal wind velocity from the Doppler radial component. The other two needed variables are azimuth of the radar beam and wind direction. Of these three variables, only wind direction is unknown at the operational site.

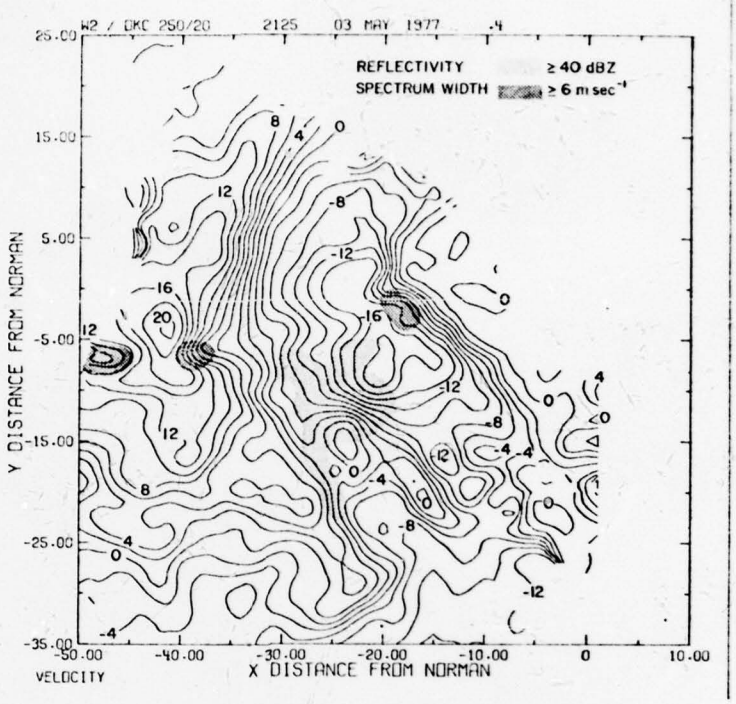

Figure 10. Doppler radial velocity contour (m s^{-1}) cross-section at 400 meters for 3 May 1977 (2125 CST) with maximum reflectivity (dBZ) and spectrum width (m s^{-1}) areas stippled.

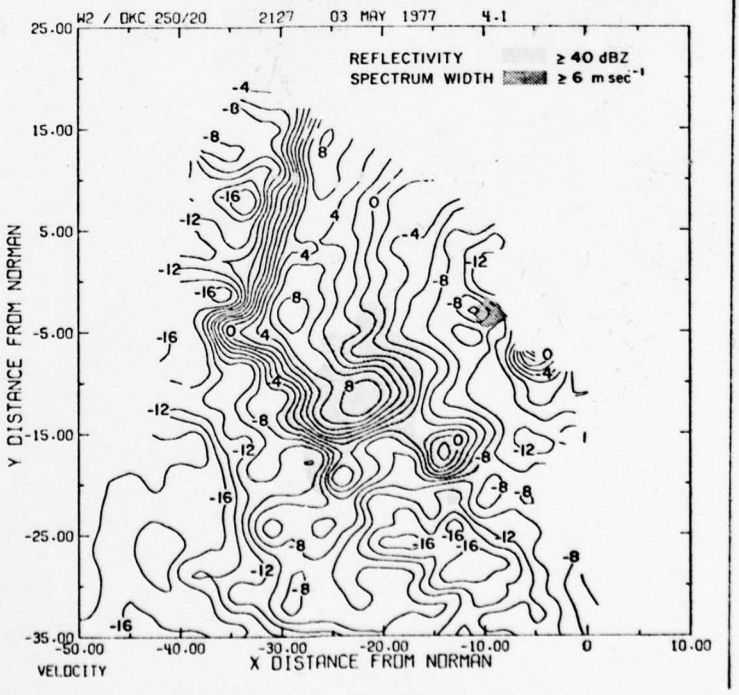

Figure 11. Same as Figure 10, but at 2127 CST and cross-section height is 4.1 km.

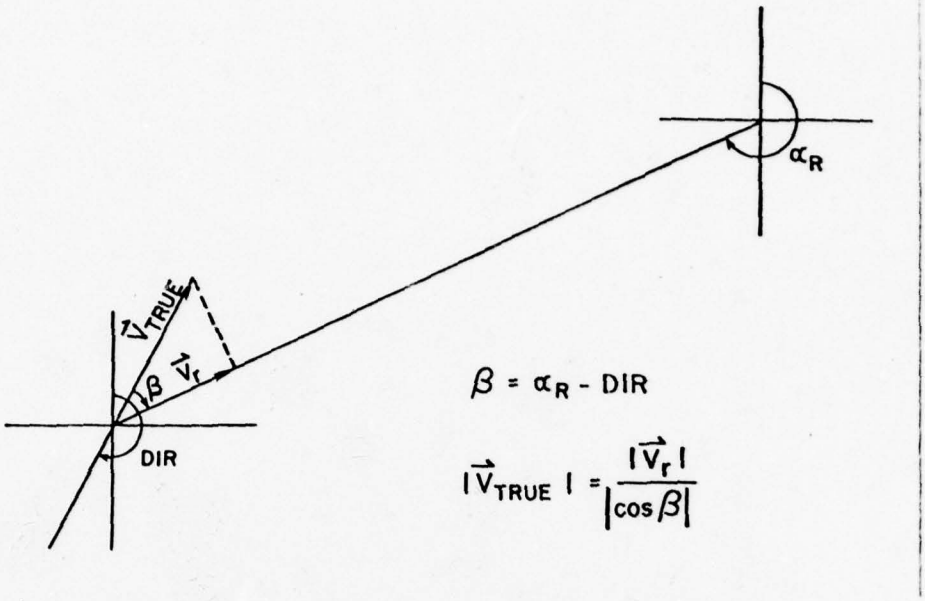

Figure 12. Radar azimuth/wind direction geometry. α_R is azimuth of the radar. DIR is horizontal wind direction. $\bar{V}_r$ is the Doppler horizontal radial wind, and $\bar{V}_{TRUE}$ is the true horizontal wind.

If the wind direction can be found with some degree of confidence, then it is possible to use this relation in an on-site minicomputer or calculator to provide true horizontal velocity winds from single Doppler data. NSSL Staff (1971) found that the "average wind direction veers steadily as the average speed increases", and as discussed earlier, a wind direction change frequently occurs prior to the gust front. The main outflow winds should occur somewhere from $+90^o$ to -90^o of the storm motion; i.e., ahead of the storm due to horizontal momentum conservation (Byers and Braham, 1949; Goff, 1976). Colmer (1971) found that the path of maximum gust on the gust front and the path of the parent cell are almost the same. Thus he states, "...if the storm track can be predicted, the track of the maximum gust can also be forecast fairly confidently...."

Although this may prove to be an oversimplification, as a first guess the wind direction will be assumed to parallel the storm motion. This approach has an initial advantage in that the AFGL echo tracking computer in place for the 1978 phase of JDOP computes storm motion and locates the maximum radial wind (Forsythe, 1978). Thus, this algorithm has been input for use and modification in real time with the on-going JDOP study.

Although the radar azimuth/wind direction geometry (refered to as radar/wind geometry) problem also affects the possibility of a high wind event being missed due to the relation of the outflow to the radar beam, no case during the 1977 portion of JDOP could be shown to have been missed due to the geometry. It is possible that this would have occurred with a larger data sample, and thus any conclusions will have to await additional data gathering efforts.

One additional effect of the radar/wind geometry is the determination of the true horizontal extent of the outflow. Assume that the high wind region (-19 m s^{-1}, yellow) in Figure 13a is outflow paralleling the radar beam. While velocity will normally be less at the edges of the outflow region, the radar/wind geometry relation will cause the Doppler radial velocity to drop off faster (Figure 12). A wind direction change or change in the height of the data will further complicate the problem. The present study simply recognizes that high winds will possibly extend beyond that area appearing on the Doppler radial velocity field and recommends this item for further research.

(a)

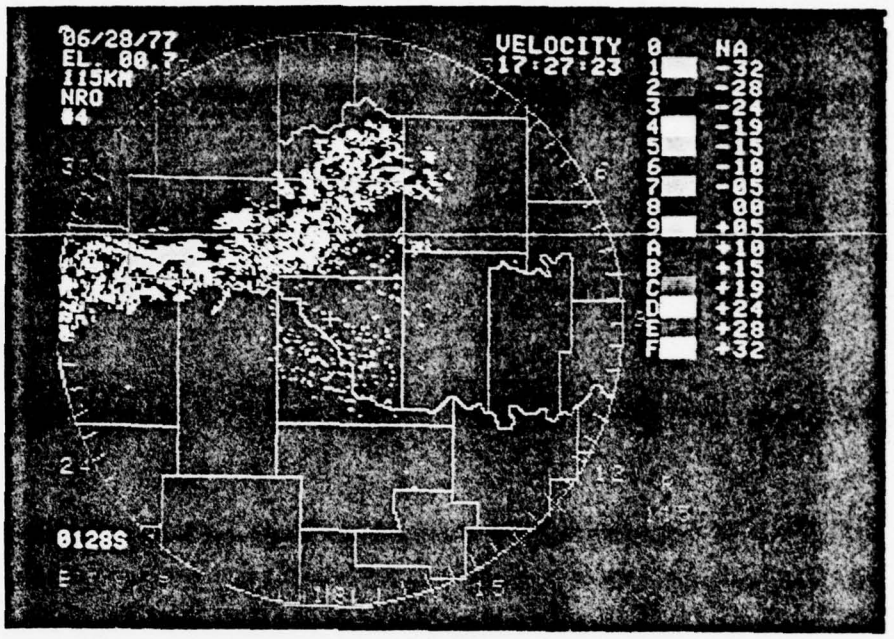

(b)

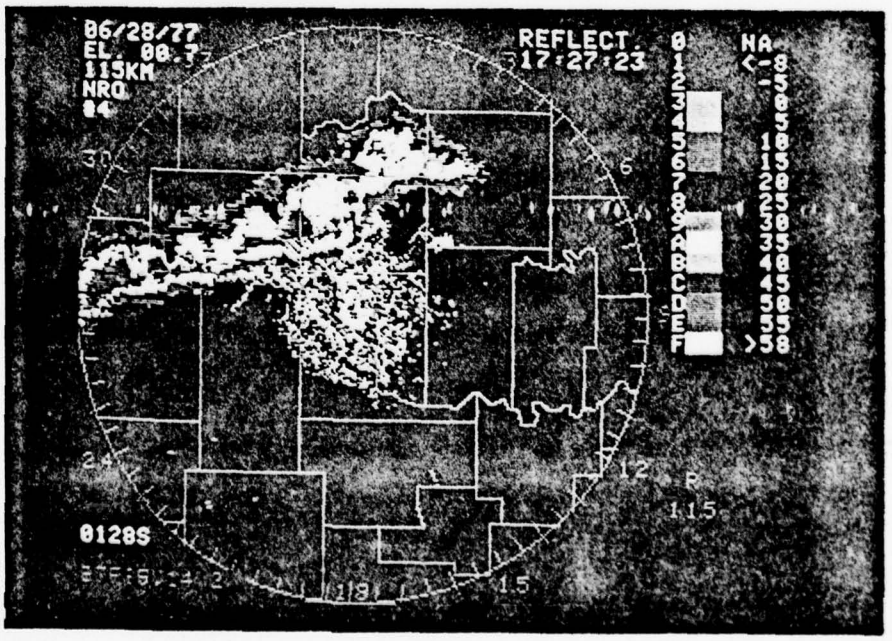

Figure 13. Doppler displays of (a) velocity (m s^{-1}) and (b) reflectivity (dBZ) for 28 June 1977 (1727 CST). Scope range is 115 km and county lines are shown.

3.5 Gust Front Examination

3.5.1 General features

Of all the data collected during JDOP (1977), the May 3rd storm was the best defined straight line wind case. A line of thunderstorms moved through the JDOP area of responsibility (Figure 14) and, more importantly, through the NSSL mesonetwork. W2 category winds were detected at 2036 CST (220°/70 km) and 20 - 25 m s^{-1} winds were monitored until they entered the radar ground clutter pattern. Broken windows and roof damage occurred in downtown Oklahoma City at 2245.

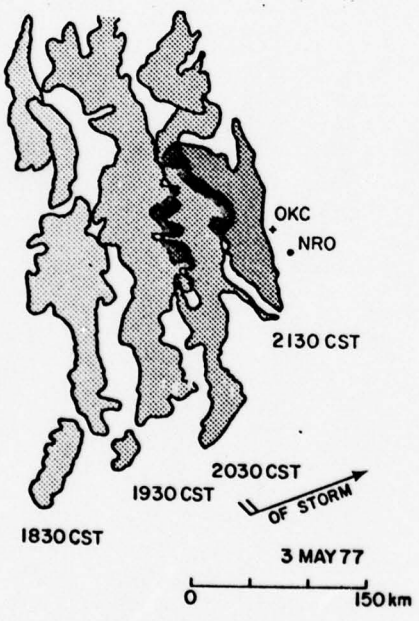

Figure 14. PPI time sequence of squall line on 3 May 1977 from the OKC WSFO WSR-57 radar.

Examination of the lowest cross-section of data available at 2125 (400 m) shows distinct features of the thunderstorm outflow over the NSSL mesonetwork (Figure 15). Seen in the single Doppler contoured radial velocity field is a sequence of windshift (A), gust surge (B),

secondary windshift (C), and second gust surge (D). This compares very well with the typical sequence of events in the gust front cases studied by Charba (1974) and Goff (1976).

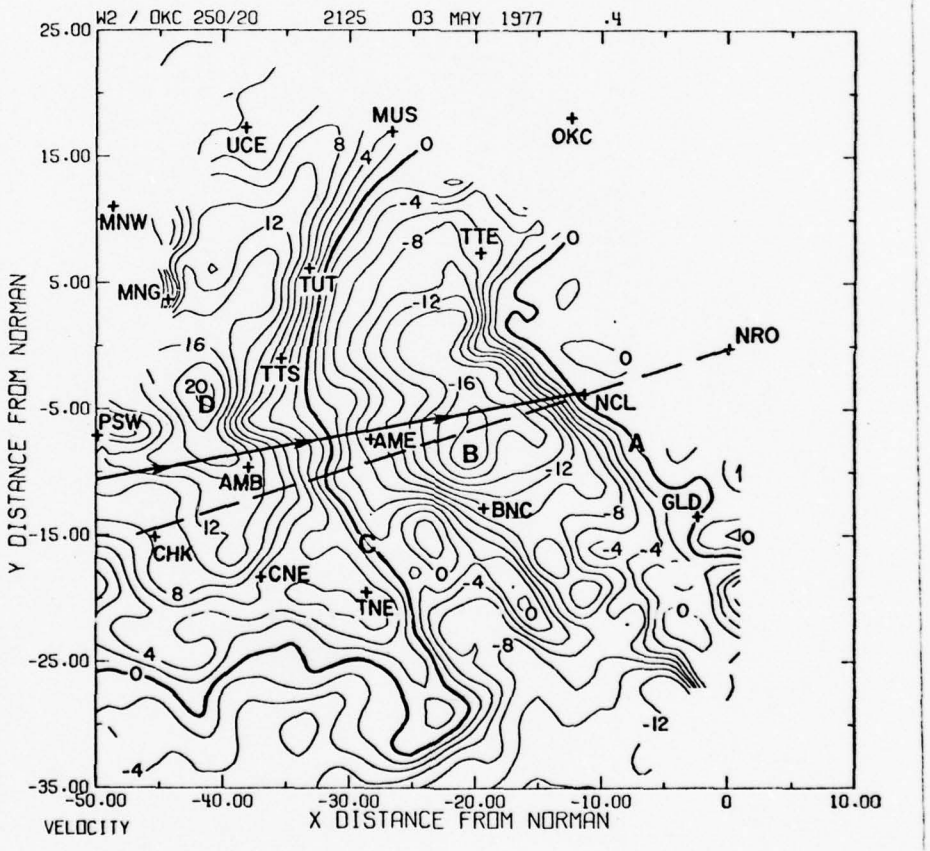

Figure 15. Cross-section at 400 m of Doppler radial velocity contours (m s^{-1}) showing gust front at 2125 CST on 3 May 1977. Mesonetwork sites are labeled with three letter identifiers. Storm motion is shown as arrows and vertical cross-section as dashed line. Single letters refer to features discussed in text.

The mesonetwork gave quite detailed surface verification. While data from all surface sites were examined, data from the Newcastle (NCL) site (Figure 16) illustrate additional details of this gust front.

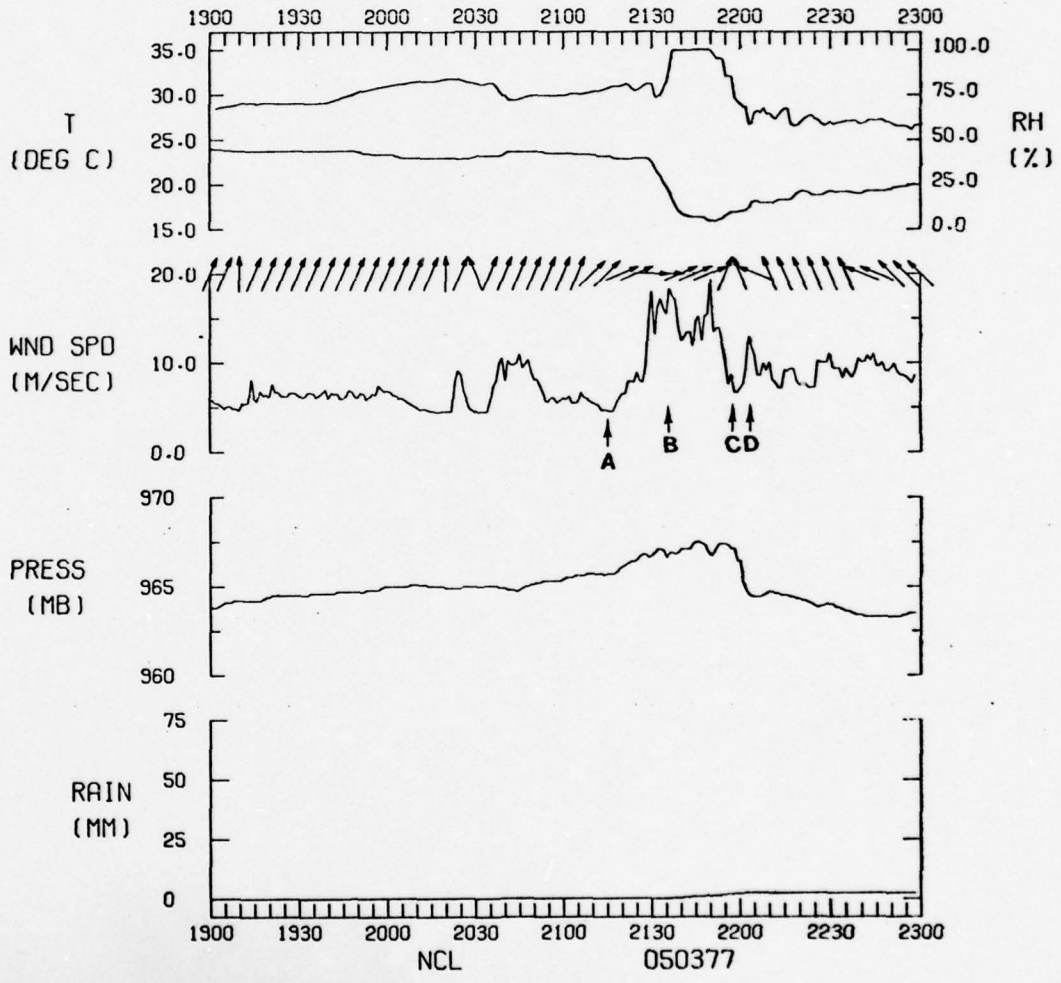

Figure 16. Analog plot to surface strip chart for Newcastle (NCL) mesonetwork site for 3 May 1977. (Letters refer to features discussed in text and identified in Figure 15.)

The pressure jump as seen by Charba (1974) does not appear. Instead, a slow pressure rise, similar to that in the cases studied by Goff (1976),

can be seen beginning at about 2045. The rate of the pressure rise increases near 2115 (A) at which time there is a drop in wind velocity and wind direction begins more marked veering. Within a 10 minute period wind velocities have nearly doubled in the gust surge (B), and there is a very evident temperature break and drop in relative humidity. From this information it is surmised that the gust front reached the NCL surface site at 2115 and the main body of the cold air outflow arrived by 2130. A strong wind shift (C) and its associated drop in wind speed coupled with a 6 mb pressure drop followed this air mass. The pressure drop was seen to some degree at all of the mesonetwork sites and corresponds to a "wake depression" (Fujita, 1955; Williams, 1963). A second wind surge (D) followed this wake depression.

Figure 15 presents a classic picture of diverging flow. The air mass to the right of the wind shift line (C) is flowing toward the radar and the air mass to the left of this line is flowing away from the radar. This excellent example of a single Doppler line divergence pattern leads to the idea that the downdraft of the thunderstorm may be flowing down and forming the low level outflow in the vicinity of this windshift (C). To examine this further requires information from the upper levels of the storm.

3.5.2 Vertical cross-section

Five elevation angles were used in the tilt sequence on May 3rd during the time that the gust front was traveling through the NSSL mesonetwork. The five corrected elevation angles (1.0, 3.0, 4.8, 7.0, 9.0) provided data that have been combined into a single vertical cross-section along a radial from the radar.

Figure 17 shows the reflectivity and radial velocity in the vertical cross-section that lies through the Newcastle (NCL) mesonetwork site (252.3° radial). It should be noted that the radar did not "top" the storm, but that some quite interesting features are apparent in that portion of the storm being viewed.

(a)

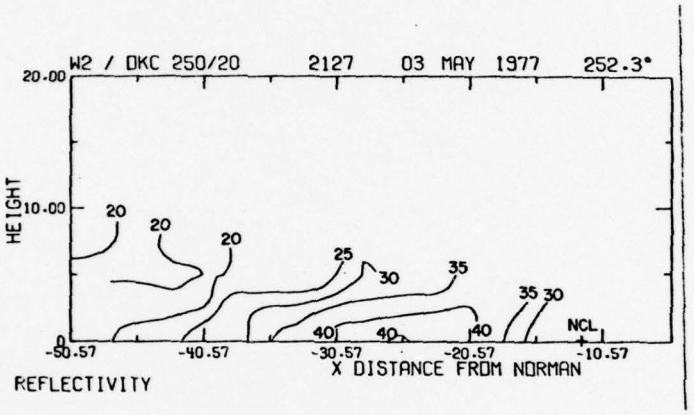

(b)

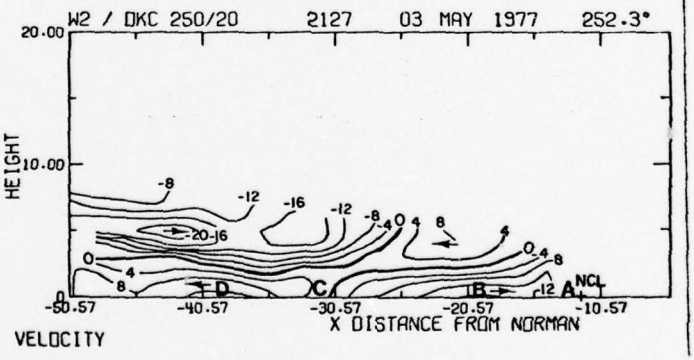

Figure 17. Vertical cross-section along 252.3° radial (through Newcastle mesonetwork site, NCL). Doppler (a) reflectivity (dBZ) and (b) radial velocity (m s^{-1}) at 2127 CST on 3 May 1977. (Letters refer to features discussed in text and identified in Figures 15 and 16. Arrows show air motion relative to the radar).

The flow patterns look very much like those used by Goff (1976) (Figure 2) in his outflow studies. Cold air outflow appears at the low levels (surface to 3 km) moving toward the radar below apparent warm air inflow (above 3 km) moving away from the radar. A very strong inflow can be seen at the midlevels (5 km) back of the reflectivity core. "Wake flow" (flow into the thunderstorm wake) can be assumed from the positive velocity region at the low levels (surface to 3 km) behind the high reflectivity region. The cold air outflow (Figure 17) appears deeper than that seen in the cases reported by Charba or Greene et al. (1977). This difference may be a function of where the outflow is measured. As seen in Figure 2, the outflow depth in the first surge, measured at its present position well out from the parent cell, will not be as deep as the most recent surge, shown close to the rain shaft. In the case studied by Charba (1974) the maximum cold air outflow depth was 1.7 km and the mean was 1.35 km. In the cases studied by Greene et al. (1977) the outflow is reported to usually be no more than 2 km deep. Goff (1976) concludes that "the whole vertical extent of the outflow has not been observed" and only reports the depth of the "nose" of the gust front to be less than 200 m deep in the twenty cases analyzed. In this May 3rd case the convention can be adopted to measure the outflow depth within 10 km of the surface divergence (apparent position where the downdraft turns horizontal). In this case the outflow would hold a minimum depth of 3 km. Kropfli and Miller (1975) have used a multiple Doppler network to develop a three dimensional wind field in a thunderstorm, and their schematic representation of this flow shows similar inflow/outflow patterns and depths as this May 3rd case seen by single Doppler.

The divergence pattern appears with vertical continuity from the surface to 3 km. Above 3 km is a region of convergence. From the pattern of convergence and divergence presented in Figure 17, it is apparent a downdraft does exist and can be located at the surface near the reference point C. The downdraft source would appear to be located in the dry air inflow at the 5 km level on the back side of the storm. One would suspect that this is the source of the downdraft as the introduction of dry air into the storm will result in evaporative cooling, and the cooled air will sink due to resulting negative buoyancy. If there is horizontal momentum conservation in the downdraft, this air would then impact the ground at reference point C and become outflow moving toward the radar (e.g., winds around reference point B).

3.5.3 Downdraft source

There is frequent discussion in the literature regarding horizontal momentum conservation from the mid-levels of a storm to the outflow region at the surface (Byers and Braham, 1949; Walters, 1975; Goff, 1976). Having identified the downdraft at 2125 through the single Doppler velocity data, this case should be ideal to test this horizontal momentum conservation theory.

The conservative properties of equivalent potential temperature (θ_e) make it an excellent tracer. θ_e was computed for all of the mesonetwork sites at 2125 and plotted in Figure 18. As can be seen, an area of minimum θ_e was located around the Amber East (AME) site where θ_e was computed as 320.1°K. The OKC sounding for 1800 was plotted using a skew T-log p chart (Figure 19), and the minimum θ_e (318.1°K) was found to occur in a layer around 600 mb. Since some mixing is

inevitable, this would appear to be the source of the downdraft air. Coupled with the previous observation from the Doppler velocity data, this θ_e connection establishes rather conclusively that the downdraft at 2125 reached the ground just forward of the wind shift line (C) and behind the gust surge (B).

If horizontal momentum conservation is to hold, then the horizontal winds at the downdraft origin and the surface winds at AME should show comparable direction and speed. However, since wind speeds may differ due to gravitational accelleration, pressure differential effects,

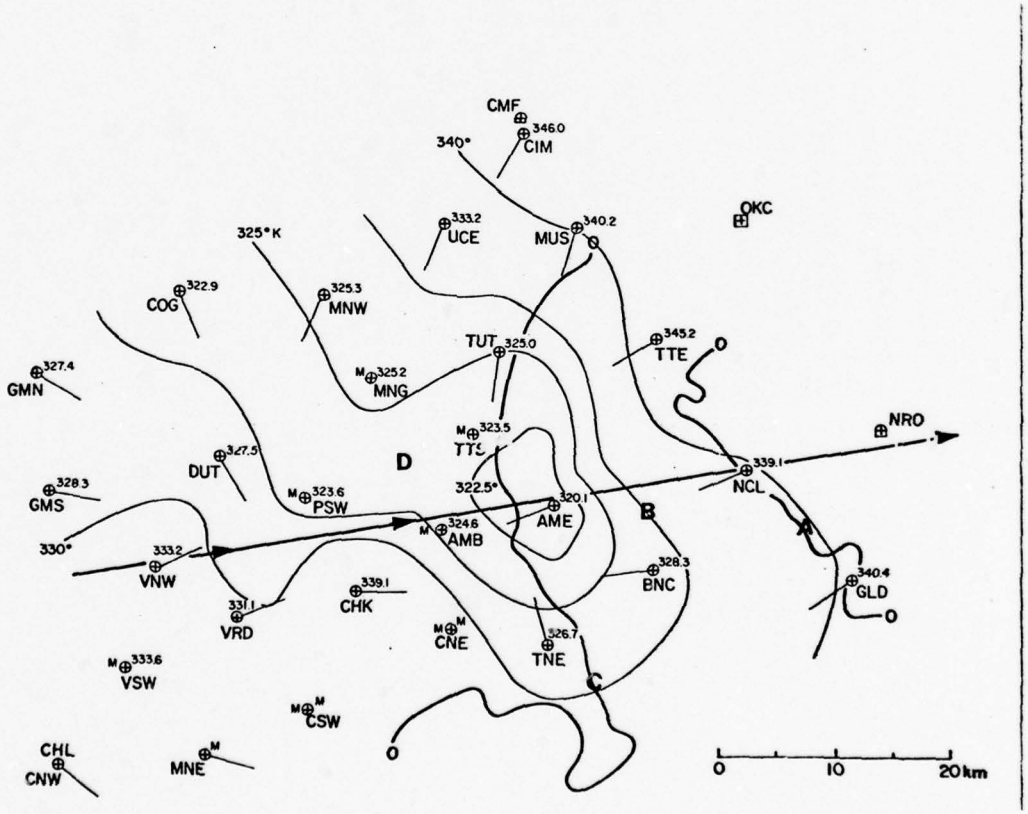

Figure 18. Surface plot of θ_e computed from mesonetwork data on 3 May 1977 at 2125 CST. Letters identify features discussed in text and seen in Figures 15 through 17. Storm motion is represented by arrows. Two Doppler zero radial velocity contours (wind shift lines A and C) are shown, and surface wind direction is plotted at each mesonetwork site.

friction effects and others, the comparison was made for wind direction only. Sounding winds demonstrate classical veering with height, and from the minimum θ_e layer the winds exhibit directions of 245° to 285°. The three minute average wind direction (centered on 2125) at AME is 247.5°. Since wind direction is recorded by 16 compass points, this could vary by ±22.5°. While not a perfect match with the winds at the downflow origin, the comparison is strong enough to support the theory of horizontal momentum conservation.

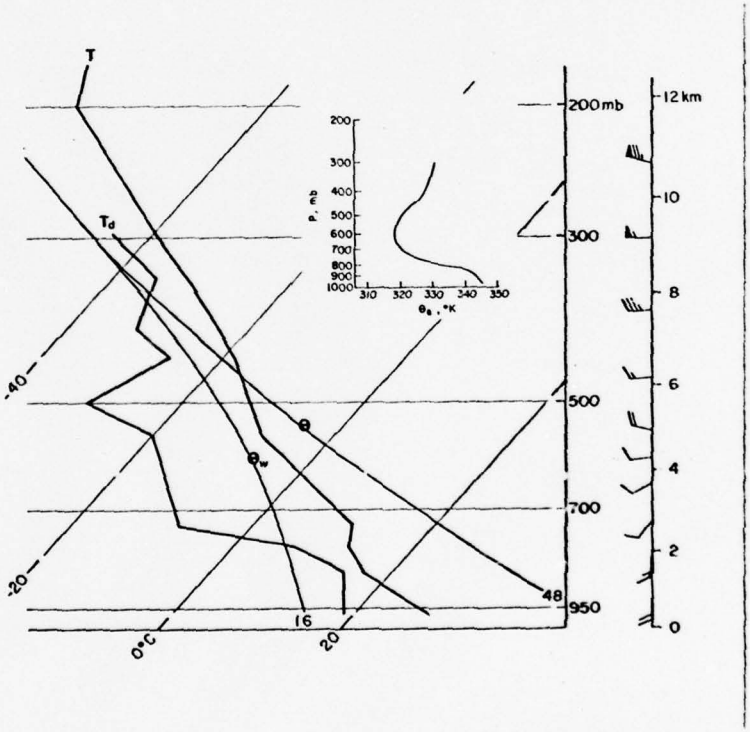

Figure 19. Sounding data from Oklahoma City at 1800 CST on 3 May 1977 plotted on a skew T-log p chart. Representative sounding winds (half barb=2.5m s^{-1}; full barb=5m s^{-1}; flag=25 m s^{-1}) are plotted with heights given in kilometers. Insert shows plot of θ_e computed from the sounding.

An additional feature of Figure 18 is the surface wind pattern. It appears that the downdraft core reached the surface within the 322.5°K θ_e contour and then diverged horizontally much like the "fluid jet striking a flat plate" described by Byers and Braham (1949). Recently the concept of "downburst" has been introduced by Fujita and Byers (1977) and Fujita and Caracena (1977). No cases during JDOP were recognized as "downbursts", but future examination of the JDOP data set may provide additonal information for study.

3.6 Data Comparisons

3.6.1 Timing study

Since verification of what the single Doppler radar sees is available only at the surface, one must consider the changes in the outflow from the height of the radar cross-section to the surface. Unfortunately, the reasons for these changes are largely unknown and await further study for complete definition.

The first attempt to examine this change in the outflow involved timing the passage of identifiable events across the NSSL mesonetwork. If the contoured single Doppler radial velocity data (Figure 15) are assumed to be steady state and all the features are assumed to be moving with storm motion, one can compare time of event occurrence at a mesonetwork site based on Doppler data to time of actual occurrence seen on surface strip charts.

Storm motion was developed from Oklahoma City WSFO WSR-57 scope overlays (Figure 14) and scope photography, and NSSL radar scope photography. Once storm motion was determined, a direction line was drawn through each mesonetwork station on the Doppler radial velocity contours,

and identifiable features were selected from this contour field. The May 3rd case (Figure 15) shows readily identifiable sharply increasing velocity gradient (directly following A), a peak wind (B), a wind shift (C), and a second wind peak (D). The distance along the storm direction line to each of these features was measured from each station and recorded These features were then identified on the strip charts from the surface mesonetwork sites (e.g., Figure 16), and occurrence times were recorded.

Using the distances from the Doppler contours and the velocity of the storm, a distance-to-time conversion was made. This conversion was done last to avoid biasing the time determinations from the surface data. For example, the peak wind (B) is 8.7 km from NCL. This converts to 14 minutes and is referred to as the observed "time-to-event" based on Doppler ($\tilde{x}$). For AME the time to this same event is -14 minutes; that is, the event had taken place 14 minutes prior to the reference time (the time the radar cross-section was obtained, 2125). Subtracting this reference time from the occurrence times given by the surface strip charts provides the observed "time-to-event" based on surface data ($\tilde{y}$). For the above two examples, $\tilde{y} = 2136 - 2125 = 11$

and $\tilde{y} = 2120 - 2125 = -5$

Having obtained these pairs of observed times to specific events ($\tilde{x}$,$\tilde{y}$), the goal was to use the Doppler "time-to-event" to predict the actual event occurrence time (y).

Defining:
y = Estimate of "Time to Event (Surface)"
$\tilde{y}$ = Observed "Time to Event (Surface)"
x = Estimate of "Time to Event (Doppler)"
$\tilde{x}$ = Observed "Time to Event (Doppler)"

A Functional can be written with the form:

$$J = \Sigma[(y - \tilde{y})^2 + (x - \tilde{x})^2]$$

If it is assumed that there is no error in x, then $x = \tilde{x}$; and

$$J = \Sigma[(y - \tilde{y})^2]$$

Assume that the estimate of y is given as a linear relation to $\tilde{x}$.

$$y = m\tilde{x} + b$$

Then $$J = \Sigma[(m\tilde{x} + b - \tilde{y})^2]$$

Since it is desired to minimize the error, the first variation is taken of J and set equal to zero. This yields

$$b = \frac{\Sigma\tilde{y} - m\Sigma\tilde{x}}{N}$$

$$m = \frac{\frac{\Sigma\tilde{x}\Sigma\tilde{y}}{N} - \Sigma\tilde{x}\tilde{y}}{\left(\frac{\Sigma\tilde{x}}{N}\right)^2 - \Sigma\tilde{x}^2}$$

These terms are the slope (m) and y-intercept (b) of the "least-squares fit" line through the data.

A computer program was written to take input times, plot the scatter diagram of "Time to Event (Doppler)" versus "Time to Event (Surface)", and compute and draw the best-fit regression line from the above equations. Figure 20 shows the results for 3 May 1977 at 2125.

While the high correlation coefficient reflects the obvious connection between what the radar views 400 m above the ground and what occurs at the surface, the regression line may provide a bit more information through its slope and y-intercept.

If the regression line has a slope of 1.0 and a y-intercept of 0.0, then the conclusion would be that timing of the events was the same whether viewed by the radar above the ground or by surface observation. The change in y-intercept with the slope held constant (Figure 21a)

appears due to some timing error common to the entire data field, such as the height above the ground, a surface inversion, or surface friction.

The difference in slope is seen as a reflection of the error in the assumed speed of the event. Since time equals distance divided by speed, or

$$\Delta T = \frac{\Delta X}{C}$$

Then on the x-axis, ΔT(Doppler) equals the distance the feature must travel (measured on the single Doppler contour field) divided by the assumed speed of the feature. Although the ΔT(surface) was obtained directly, it is actually the true distance the feature traveled divided by the true speed of the feature. Thus, the slope of the regression line is

$$m = \frac{\Delta T(\text{surface})}{\Delta T(\text{Doppler})} = \frac{\Delta X(\text{true})}{C(\text{true})} \frac{C(\text{assumed})}{\Delta X(\text{Doppler})}$$

Since at the range concerned even a large direction error results in a relatively small distance error, the assumption can be made that Δx(true) and Δx(Doppler) are the same since the same distance must be covered regardless of the viewing perspective. Now it is quite apparent that a change in the slope from that of 1.0 appears due to a speed error (Figure 21b); i.e., the true event motion is not equal to the assumed speed, in this case storm speed. A slope greater than 1.0 says that the assumed speed is too fast and a slope less than 1.0 says that the assumed speed is too slow.

Although based on a limited amount of data, both ideas agree with physical reasoning. Unless the outflow feature was deep enough to be at the ground and at the radar cross-section height, one would expect

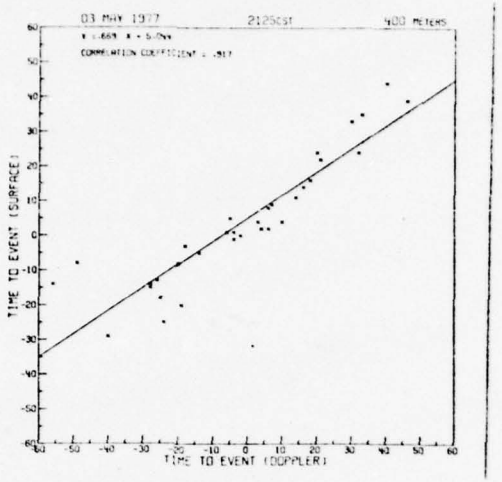

Figure 20. Scatter diagram of timing data from gust front on 3 May 1977 (2125 CST) giving equation for regression line and correlation coefficient.

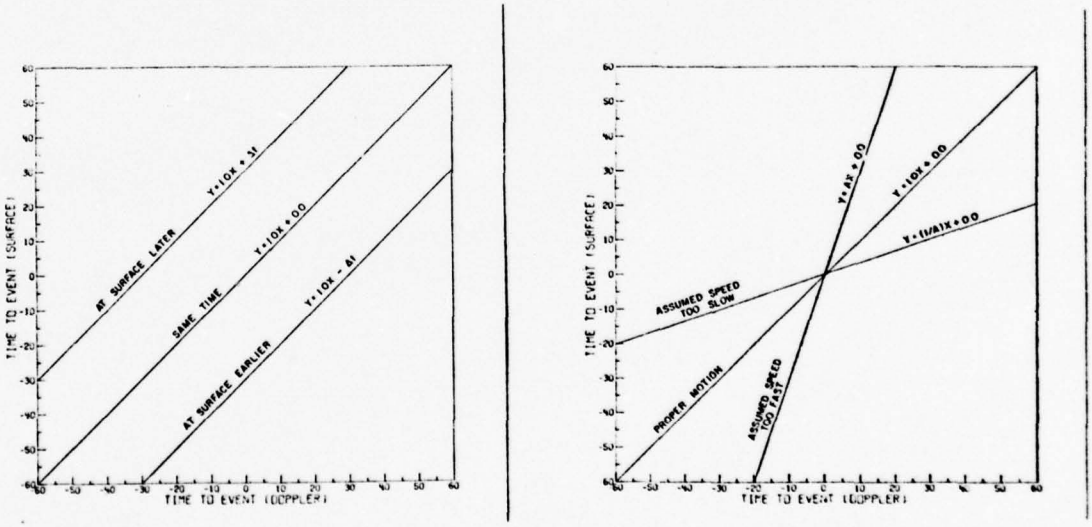

(a) (b)

Figure 21. Explanation of information obtained from the regression line in Figure 20 showing effect of (a) y-intercept and (b) slope.

a time lag (positive y-intercept) before the outflow impacts the ground. With a surface inversion, the time delay may be quite long, and the outflow may never reach the surface (Goff, 1976). The second idea is even easier to approach as it is fully expected that the outflow (gust front) will propagate out away from the parent thunderstorm cell. Thus, a slope of less than 1.0 would be expected. The May 3rd case, a well-defined gust front, exhibits these very features. As can be seen in Figure 19, there exists a positive y-intercept indicating a 5 minute time lag from the forecast occurrence time based on the Doppler information and the actual occurrence determined from surface data. The slope (.669) implies an error in the assumed horizontal translation speed of the features. While it was assumed that the features were moving at 10 m s^{-1}, they were in fact moving at 15 m s^{-1}. In one hour the gust front would have moved 18 km ahead of the parent cell. This is in good agreement with Goff (1976) who has shown that the gust front average speed will typically be 11.3 m s^{-1} for quasi-steady outflow to 18 m s^{-1} in final stage of the life cycle.

3.6.2 Surface versus Doppler wind study

Once the regression line is known, the error for a given Doppler timing value can be computed between the point on the regression line and the observed surface timing value. With enough data points this error can be taken to have a normal distribution.

With the assumption of a normal distribution and the computation of the standard deviation of the error, it is possible to compute the confidence interval (Lentner, 1972). Thus, given a value of the time to the event occurrence from the Doppler, it can be stated with a given

percent probability that the actual event took place, or will take place, at the time computed from the regression line plus or minus a certain number of minutes. For example, on 3 May 1977 (2125 CST), there is 80 percent probability that the event occurred at the time given by the regression line plus or minus 9 minutes. There is 50 percent probability that the event occurred at the time given by the regression line plus or minus 5 minutes.

These confidence intervals were used to compare peak winds. The peak wind that appears to affect a surface station was noted from the Doppler data, and the time to this occurrence was derived as before. The regression line was used to predict a surface occurrence time, and from the confidence limits a time range was obtained. The strip chart for this station was examined and the peak wind within this time range recorded. This peak true wind was compared with the peak Doppler radial wind. Then, given the surface wind direction and radar azimuth to the mesonetwork site, the surface peak wind was converted into a radial peak wind and compared with the Doppler radial peak wind.

This comparison also used the "least-squares" best-fit approach. The results for the May 3rd case show little correlation between the absolute value of the Doppler peak radial velocity and the surface peak velocity for each mesonetwork site. When the radial component derived from the surface peak velocity is compared with the Doppler peak radial velocity a strong correlation results. More significant than this correlation is the mean error of the peak wind measurement. When using the 50 percent confidence interval, the mean error of the peak Doppler radial component as an estimate of the peak surface wind was only 3 m s^{-1}.

When the radial component derived from the peak surface wind was compared with the peak Doppler radial component, a mean error of 5 m s^{-1} was obtained. When the estimate of peak surface wind was derived from the Doppler peak radial component and the regression equation (least-squares best-fit line), the mean error was 3 m s^{-1}.

The data set used here was extremely small, but the implication is that the averaging done by the radar and the analysis routines is enough to smooth out the extreme wind values (the wind peaks), but not so much as to seriously bias the data (mean error of 3 - 5 m s^{-1}).

The examination of peak winds involved selection of data from different times. Two additional data sets were examined by comparing wind magnitudes at common times.

The first was the comparison of surface wind velocity versus the absolute value of the Doppler radial velocity. As with the peak winds, poor correlation was shown, and the mean error of 5 m s^{-1} was no better than that found with the peak winds.

The second comparison was that of surface radial velocity versus Doppler radial velocity. Again, like the peak winds, data in this case showed a strong correlation and a mean error of 3 m s^{-1}. When the surface winds were estimated by the Doppler radial winds and the regression equation for this data, the mean error dropped to 2 m s^{-1}. While any conclusions must be viewed in light of the limited data set, it would appear that winds seen by the radar 300 to 500 meters above a point on the ground do represent the surface wind at that point reasonably well (mean error of 2 - 5 m s^{-1}). The conclusion of Greene et al. (1977) that "wind measurements near the ground often do not represent

true gust-front intensity or movement" may account in part for this error Regardless of the error source, this analysis indicates that low level Doppler data does give a good representation of those winds recorded at the surface.

3.6.3 Future technique improvement

While the assumption was initially made that $x = \tilde{x}$, it was subsequently shown that the assumed speed did not equal the true speed ($x \neq \tilde{x}$). With $x \neq \tilde{x}$ and the functional in the form of

$$J = \Sigma[(y - \tilde{y})^2 + (x - \tilde{x})^2]$$

the estimate of y must be given as either $y = m\tilde{x} + b$

or $y = mx + b$

Using the first,

$$J = \Sigma[(m\tilde{x} + b - \tilde{y})^2 + (x - \tilde{x})^2]$$

and setting the first variation equal to zero yields three equations and three unknowns. Two of the equations yield "m" and "b" in the same form as the original ($x = \tilde{x}$) development. The third equation reveals that

$$\Sigma x = \Sigma\tilde{x}$$

but this does not seem to provide a useful basis for further analysis.

The second possible form of the relation of y to x yields a functional in the form

$$J = \Sigma[(mx + b - \tilde{y})^2 + (x - \tilde{x})^2]$$

Setting the first variation equal to zero also yields three equations and three unknowns. Two of the equations provide "m" and "b" in the form of the original with x in place of $\tilde{x}$. However, x is also an unknown. The third equation merely simplifies into

$$\Sigma x = \Sigma\tilde{x}$$

Developing a solution to this dilemma is outside the scope of this study, and only subjective comments can be offered. This functional, once solved, should provide a more accurate method of estimating the time of occurrence of a wind event at a surface site based on the Doppler information. Although at the low levels the lead time provided would likely be only a matter of minutes, it is possible that with modification this approach could be used at the mid-levels and thus extending the lead time to an operationally significant interval.

Once the proper form for the functional is established, the next step would be to develop weighting functions to "fine tune" the forecast. Thus, the function might appear as

$$J = \Sigma[\tilde{\alpha}(mx + b - \tilde{y})^2 + \tilde{\beta}(x - \tilde{x})^2]$$

It would seem logical that the weighting functions might be a function of storm motion, height of the radar cross-section, storm tops, and environmental sounding data (perhaps wind direction at the 4 to 6 km level). In a similar fashion the "type" of storm might cause a change in a weighting function, as we would expect dynamic differences in the squall line, frontal system, and single cell situations (NSSL Staff, 1971).

4. SUMMARY AND CONCLUSIONS

Continued work with Doppler radar needs to be done in the area of non-mesocyclone related gust fronts. This was but the first step toward development of an operational wind signature.

From real-time observations, it is apparent that even without a sophisticated wind signature, wind advisories can be issued with a high measure of skill. The examination of advisory skill during the 1977 phase of JDOP shows that the correlation between surface data and radar data obtained in the atmosphere's lowest kilometer is greater than that for radar data obtained above 1 km. Thus, until additional research is done, the Doppler radar will be most successful in advising on low level outflow winds inside a range of 115 km.

No significant patterns were found in the low-level Doppler composites of reflectivity, velocity, and spectrum width. However, examination of additional mid-level composites, low-level and mid-level composites as a set, and composites on a time sequence basis might prove worthwhile. The position of features at a single time do not appear significant, but the movement or development of these features might provide an operational tool for wind advisories.

A simple trigonometric relationship can be used with Doppler radial velocities to derive a true horizontal wind when some estimate of the wind direction can be found. The use of wind direction paralleling storm motion appears to be a valid first guess, but this remains to be tested and refined in a future study. The effect of radar/wind geometry on representation of the horizontal extent of the outflow is recognized as a possible problem, but additional study will be necessary to clarify

its impact on real-time operations.

The classic gust front features of the May 3rd storm provided detailed comparison of Doppler radar data to surface mesonetwork data. The horizontal radial velocity cross-section 400 m above the ground shows a sequence of wind shift, wind surge, second wind shift, and second wind surge. This appears as a classic single Doppler line divergence pattern. The vertical cross-section clearly shows the low-level cold air outflow and wake flow, and the dry air inflow in the mid-levels. From this information a position for the downdraft was derived. With an apparent downdraft in the mesonetwork, an analysis was done using equivalent potential temperature to test the theory of horizontal momentum conservation in the downdraft. Using θ_e, downdraft origin was located in a layer near the 600 mb level. The good comparison between wind direction at this level and the surface supports the momentum conservation theory.

Examination of event timing illustrates the time lag between features seen above the ground by the radar and their actual occurrence at the surface. However, the regression equation derived in this study does not provide the necessary lead time for operational advisories. It is possible that operationally useful lead times might be obtained by using a similar technique to correlate data from the mid-level of the storm with the low level data and then the surface. The radar/surface timing comparison also showed outflow propagation away from the parent thunderstorm.

The various comparisons done between Doppler radial velocity data and measured surface winds show that wind data seen by the Doppler

with the radar beam centered 300 to 500 meters above the surface is a very good representation of those winds recorded at the surface.

5. REFERENCES

Armstrong, G. M. and R. J. Donaldson, 1969: Plan shear indicator for real-time Doppler radar identification of hazardous storm winds. J. Appl. Meteor., 8, 376-383.

Atlas, D., 1963: Radar analysis of severe storms. Meteor. Monogr., 5, No. 27, 177-220.

Brandes, E. A., 1975: Severe thunderstorm flow characteristics revealed by dual-Doppler observations: 6 June 1974. Preprints, 9th Conf. on Severe Local Storms, Boston, Amer. Meteor. Soc., 85-90.

_____, 1976: Gust front evolution in severe thunderstorms: Preliminary investigation with Doppler radar. Preprints, 7th Conf. on Aerospace and Aeronautical Meteor., Melbourne, Amer. Meteor. Soc., 56-61.

_____, 1977: Gust front evolution and tornado genesis as viewed by Doppler radar. J. Appl. Meteor., 16, 333-338.

Brown, R. A., L. R. Lemon, and D. W. Burgess, 1978: Tornado detection by pulsed Doppler radar. Mon. Wea. Rev., 106, 29-38.

Burgess, D. W., 1976: Single Doppler radar vortex recognition: Part I - Mesocyclone signatures. Preprints, 17th Conf. on Radar Meteor., Boston, Amer. Meteor. Soc., 97-103.

_____, L. D. Hennington, R. J. Doviak, and P. S. Ray, 1976: Multimoment Doppler display for severe storm identification. J. Appl. Meteor., 15, 1302-1306.

_____, J. D. Bonewitz, and D. R. Devore, 1978: Joint Doppler operational project: Results year 1. Preprints, 18th Conf. on Radar Meteor., Atlanta, Amer. Meteor. Soc., 442-448.

Byers, H. R. and R. R. Braham, Jr., 1949: The thunderstorm. U. S. Government Printing Office, 287pp.

Charba, J., 1972: Gravity current model applied to analysis of squall line gust front. NOAA Tech. Memo. ERLTM-NSSL No. 61, 58pp.

_____, 1974: Application of gravity current model to analysis of squall-line gust front. Mon. Wea. Rev., 102, 140-156.

_____ and Y. Sasaki, 1971: Structure and movement of the severe thunderstorms of 3 April 1964 as revealed from radar and surface mesonetwork data analysis. Jour. Meteor. Soc. Japan, 49, 191-214.

Colmer, M. J., 1971: On the character of thunderstorm gust fronts. Proceedings, International Conference on Atmospheric Turbulence, London, Royal Aeronautical Soc., 11pp.

Cressman, G. B., 1959: An operational objective analysis system. Mon. Wea. Rev., 87, 367-374.

Donaldson, R. J., Jr., 1970: Vortex signature recognition by a Doppler radar. J. Appl. Meteor., 9, 661-670.

_____, R. M. Dyer and M. J. Kraus, 1975: An objective evaluation of techniques for predicting severe weather events. Preprints, 9th Conf. on Severe Local Storms, Boston, Amer. Meteor. Soc., 321-326.

Forsythe, D. E., 1978: Personal communication.

Fujita, T., 1955: Results of detailed synoptic studies of squall lines. Tellus, 7, 405-436.

_____ and H. R. Byers, 1977: Spearhead echo and downburst in the crash of an airliner. Mon. Wea. Rev., 105, 129-146.

_____ and F. Caracena, 1977: An analysis of three weather-related aircraft accidents. Bull. Amer. Meteor. Soc., 58, 1164-1181.

Glossary of Meteorology. Edited by R. E. Huschke. Boston, Mass.: American Meteorological Society, 1970.

Goff, R. C., 1976: Vertical structure of thunderstorm outflows. Mon. Wea. Rev., 104, 1430-1440.

Greene, G. E., H. W. Frank, A. J. Bedard, Jr., J. A. Korrell, M. M. Cairns, and P. A. Mandies, 1977: Wind shear characterization. Report FAA-RD-77-33, 120 pp.

Johannessen, K., and E. Kessler, 1976: Program to develop Doppler radar for use in the National Weather Service. Preprints, 17th Conf. on Radar Meteor., Boston, Amer. Meteor. Soc., 560-561.

Kropfli, R. A. and L. J. Miller, 1975: Thunderstorm flow patterns in three dimensions. Mon. Wea. Rev., 103, 70-71.

Lemon, L. R., R. J. Donaldson, Jr., D. W. Burgess, and R. A. Brown, 1977: Doppler radar application to severe thunderstorm study and potential real-time warning. Bull. Amer. Meteor. Soc., 58, 1187-1193.

Lentner, M., 1972: Elementary Applied Statistics. Tarrytown-on-Hudson, N. Y.: Bogden and Quigley, Inc., 156-159.

Lhermitte, R. M., 1964: Doppler radars as severe storm sensors. Bull. Amer. Meteor. Soc., 45, 507-596.

Mitchell, K. E. and J. B. Hovermale, 1977: A numerical investigation of the severe thunderstorm gust front. Mon. Wea. Rev., 105, 657-675.

NSSL Staff, 1971: The NSSL surface network and observations of hazardous wind gusts. NOAA Tech. Memo. ERLTM-NSSL No. 55, 19 pp.

Smith, R. L. and D. W. Holmes, 1961: Use of Doppler radar in meteorological observations. Mon. Wea. Rev., 89, 1-7.

United States Department of Commerce, 1977: Storm data and unusual weather phenomena. Environmental Data Service, NOAA, April-June.

Walters, G. W., 1975: Severe thunderstorm wind gusts. Master's Thesis, Colorado State University, 81 pp.

Williams, D. T., 1963: The thunderstorm wake of May 4, 1961. National Severe Storms Project, Report No. 18, 23 pp.

6. APPENDIX

Daily General Summary

The following are summaries of the JDOP activities dealing only with wind advisories and high wind events. None of the verification data were known to the operational team in real-time. All the azimuth/range references are given with respect to the NSSL Norman Doppler, all times are Central Standard, and all cities referred to are in Oklahoma.

1. 3 May 1977

Convective activity, which began in the Texas panhandle and developed into a line of moderate to heavy thunderstorms during the afternoon, moved into the JDOP area of responsibility (Figure 14). At 1815 Altus AFB (247°/177 km) recorded wind gusts to 27 m s^{-1} and minor damage was sustained. At 1833 the Tipton (240°/176 km) subsynoptic site recorded gusts to 29 m s^{-1} with no reports of damage. Neither of the events were recognized and no advisories were issued. An update advisory (original issued while not "in operation") was passed to the Oklahoma City (OKC) WSFO and the base weather station at Tinker AFB (TIK) at 2139 when W2 winds were observed at 250°/20 km. Neither of these offices recorded high winds, but broken windows and roof damage occurred in downtown Oklahoma City at 2245 for a Hit to both agencies.

2. 14 May 1977

Strong thunderstorm activity developed in both northwestern and southwestern Oklahoma and moved eastward across the state. At 1746 a W2

advisory was issued for a storm 11 km southwest of Cheyenne (279°/210 km). At this range the data used for this advisory were 3.1 km above ground. Maximum winds of 15 m s^{-1} were recorded in the NSSL subsynoptic network at 1757. At 1930 damaging winds were reported at Taloga (305°/160 km), and at 2200 the line moved into the area of Anadarko (260°/67 km) causing additional wind damage. Two Misses were logged on this storm. At 2244 a W2 advisory was issued on cells 15 km WSW of Rush Springs (229°/80 km). Damaging winds occurred at Marlow (215°/80 km) at 2325. The time between advisory and damage leaves some question in the verification of this advisory. However, examination of the film and digital data leads to the conclusion that this met the criteria for a Hit.

3. 15 May 1977

Widely scattered showers and thundershowers were forecast. At 2129 a W1 advisory was issued for activity approaching Oklahoma City. No wind reports or damage confirmed this advisory (False Alarm).

4. 16 May 1977

A major shortwave approached western Oklahoma from the southwest and moderate to strong thunderstorms developed in the Texas panhandle after noon and began to move into western Oklahoma. At 1900 a W2 advisory was passed to OKC WSFO for an area 9 km north of Cheyenne (285°/200 km). At 1920 Leedy (293°/184 km) reported high winds, marble size hail, and very heavy rain. At 1943 the W2 advisory was updated for the line 9 km east of Butler (288°/160 km) to 28 km northeast of Leedy (296°/170 km). No damaging winds were reported until 2157 when 26 m s^{-1} winds occurred at

Stillwater (020°/102 km). Since advisory updates were not counted separately, this gave one Hit for the day.

5. 19 May 1977

Triggered by an intense upper level wave, a line of moderate to strong thunderstorms developed in western Oklahoma and moved eastward across the state. At 1230 Hobart (262°/150 km) recorded peak winds of 27 m s^{-1} at 1236 for a W2 Miss. At 2037 a W2 advisory was issued 9 km north of Gene Autry (158°/110 km). At 2045 damaging winds occurred in Overbrook (167°/130 km) and at 2110 winds of 26 m s^{-1} were recorded at Ardmore (166°/121 km) for a W2 Hit.

6. 20 May 1977

Very high potential for severe weather existed on this day, and JDOP operations began at 1325. Very little data was collected by the JDOP team due to multi-Doppler research operations from 1500 to 2030. A W2 advisory was issued for an area 4 km north of McCloud (050°/42 km) at 2205. There were no subsequent reports of damage from this storm (False Alarm). Post-analysis indicates surface winds in the mesonetwork in excess of 26 m s^{-1} from 2310 to 2320. As no advisory was issued, this became a Miss.

7. 30 May 1977

Showers and thunderstorms developed in northern Oklahoma and moved southward throughout the afternoon and evening. Vance AFB (END) recorded winds gusting to 22 m s^{-1}, but due to the first trip ground clutter

(Figure 1) this was hidden to JDOP. At 1830 a W1 advisory was issued for a region from 010°/45 km to 020°/45 km. This proved to be a Hit to OKC and a False Alarm to TIK. Later in the evening a strong thunderstorm developed within the mesonetwork and moved south. At 2016 a W2 advisory was issued at 271°/42 km (Figure A-1). Between 2010 and and 2100, Dutton (267°/58 km), Verden NW (258°/64 km), and Pocasset (262°/50 km) mesonetwork sites recorded winds greater than 25 m s^{-1} (Figure A-2). At 2106 the W2 advisory was updated at 260°/72 km (6 km NE Anadarko). Between that time and 2128, Verden (253°/58 km) and Cyril (247°/77 km) mesonetwork sites recorded winds greater than 25 m s^{-1}, and at 2125 Anadarko (255°/74 km) sustained wind damage. At 2206 major wind damage occurred at Lawton (231°/110 km) (Figure A-3). Unfortunately, at the time digital data was recorded the storm was obscured by first trip ground clutter (Figure 1).

8. 28 June 1977

Showers and thunderstorms developed as a weak cold front moved southward across Oklahoma. At 1631 a W1 advisory was issued, and upgraded to W2 at 1643 for a line 320°-340°/45-50 km. At 1705 the KTVY instrumented television tower (356°/37 km) site recorded 25 m s^{-1} and at 1730 gusts to 26 m s^{-1} were reported in northeast Oklahoma City. Gusts to 21 m s^{-1} were reported at OKC at 1736. Unfortunately, the mesonetwork had been secured for the season, but limited surface and tower data were available from the KTVY tower site and the North Penn (350°/47 km) surface site. The tower lost power due to a lightning strike at 1712 and no upper level data were recorded until after 1755. As the following figures demonstrate,

(a)

(b)

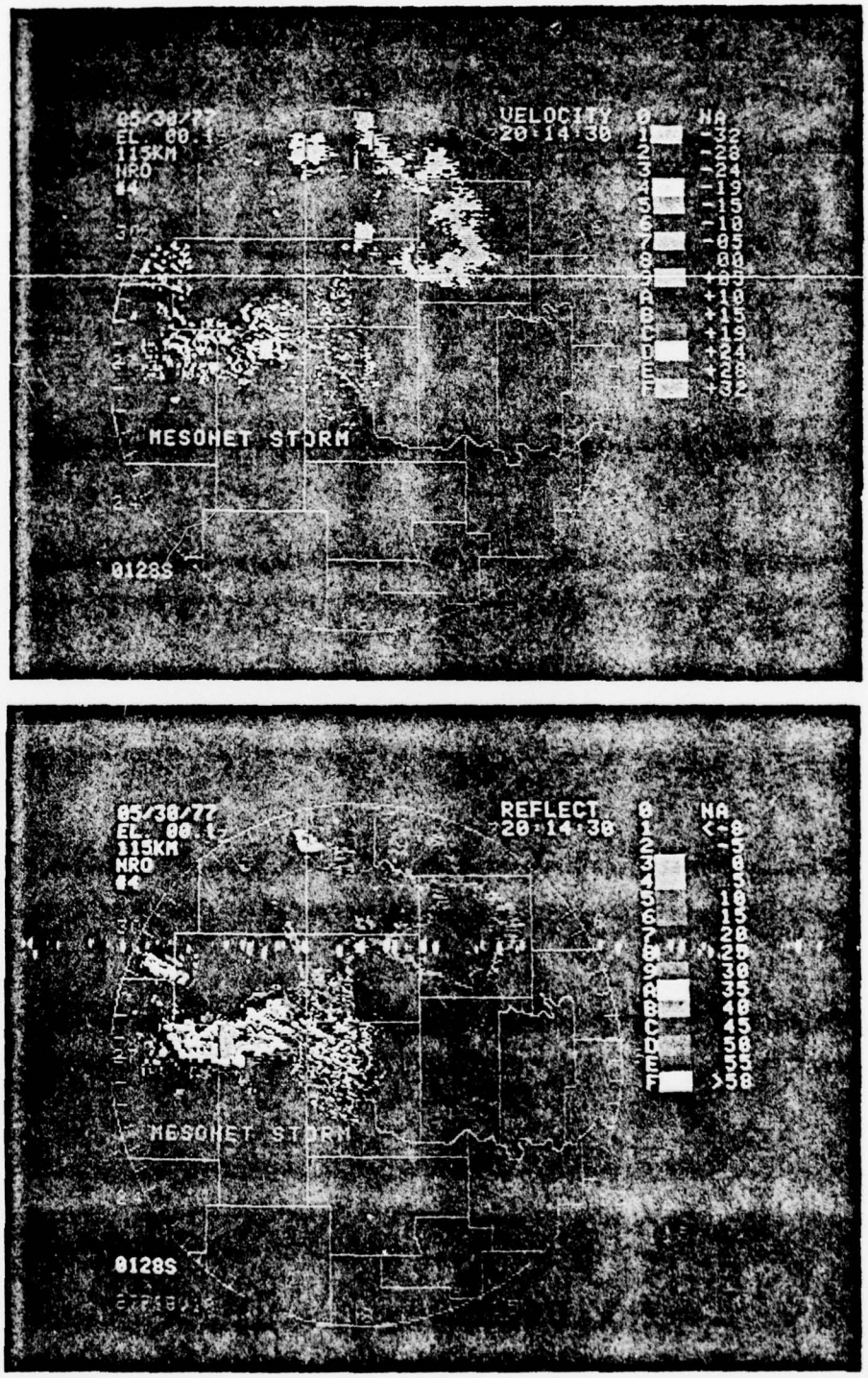

Figure A-1. Doppler displays of (a) velocity (m s^{-1}) and (b) reflectivity (dBZ) for 30 May 1977 (2014 CST). Range is 115 km and county lines are shown.

(a)

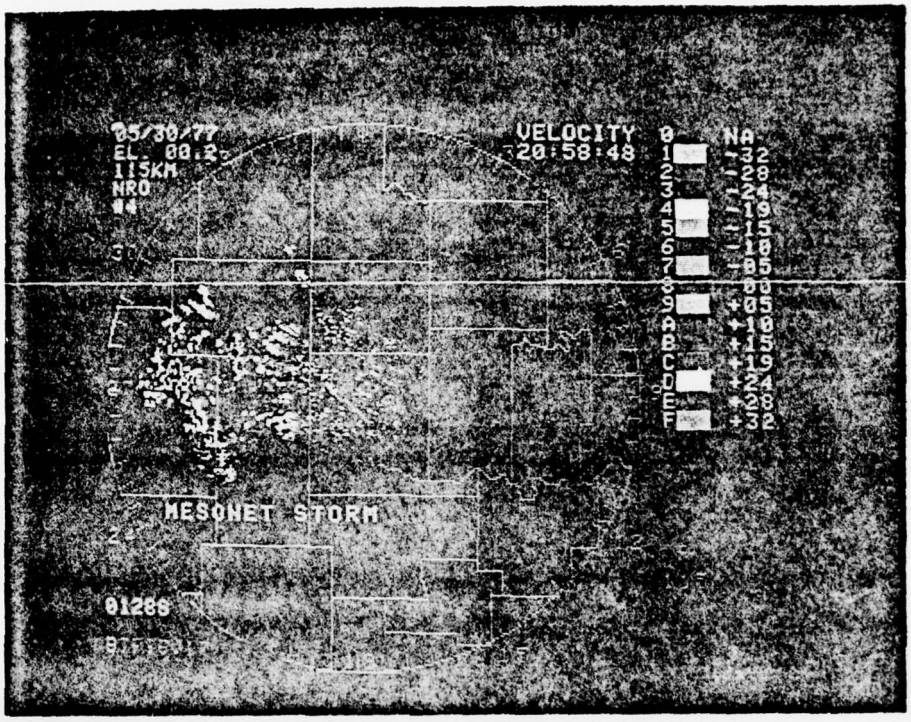

(b)

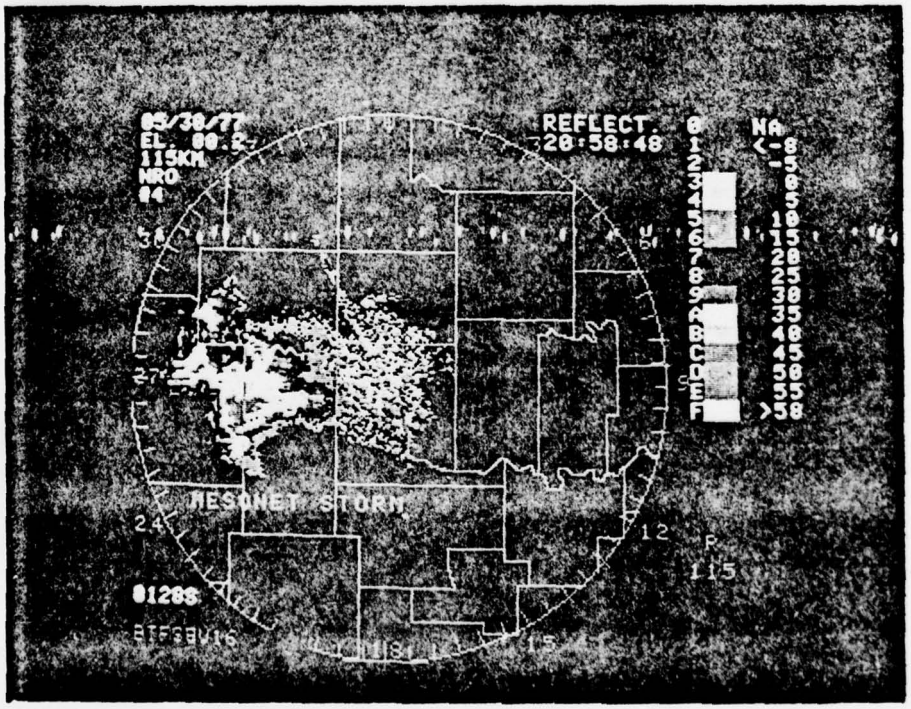

Figure A-2. Same as Figure A-1, but at 2058 CST.

Figure A-3. Straight line wind damage at Lawton, Oklahoma (30 May 1977).

this squall line case is an excellent example of the development of strong outflow winds. Although several cores have reached 50 dBZ by 1620, the winds are seen to be only on the order of 5 m s^{-1} (radial component) (Figure A-4). At 1700 the line is closer to the radar and two cells exhibit reflectivity of 50 dBZ. The outflow has become developed with an area showing radial velocities on the order of -19 m s^{-1} (yellow). Although it may be due to the radar/wind geometry, it also may be significant that these high velocities are not associated with the high reflectivity cores (Figure A-5). Using the 115 km range at 1727, maximum radial velocities are seen on the order of -24 m s^{-1} (Figure 13, dark red).

(a)

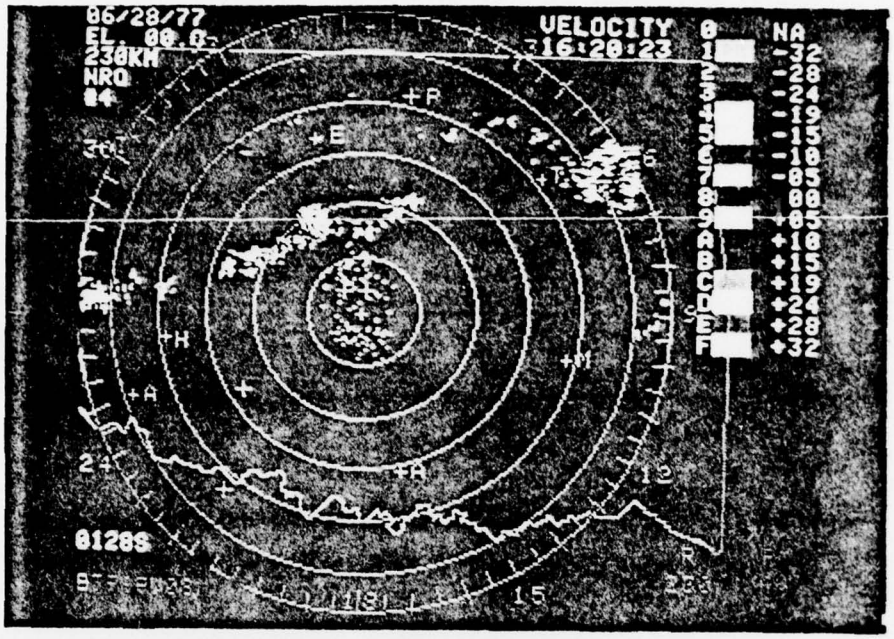

(b)

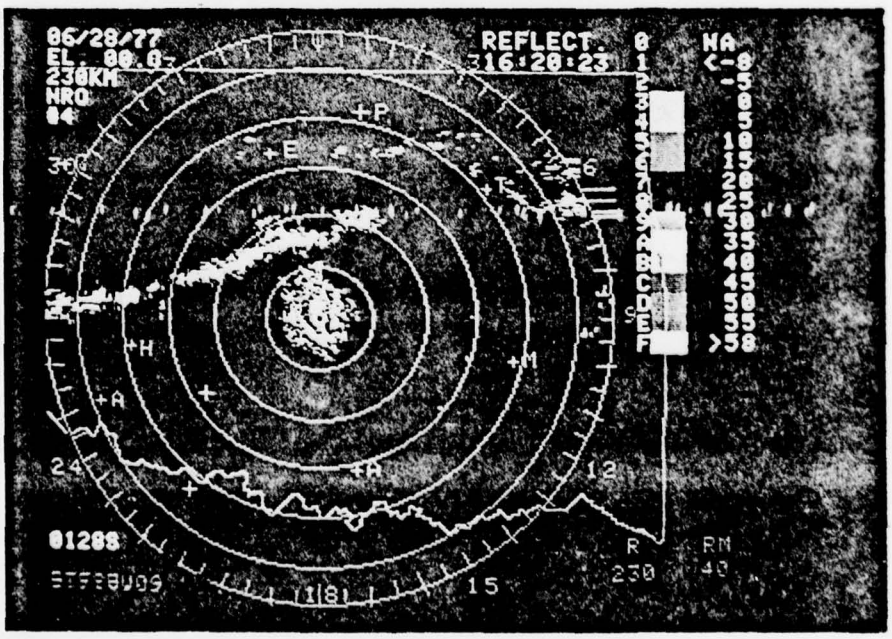

Figure A-4. Same as Figure A-1, except at 1620 CST on 28 June 1977, range is 230 km, and range marks are 40 km.

(a)

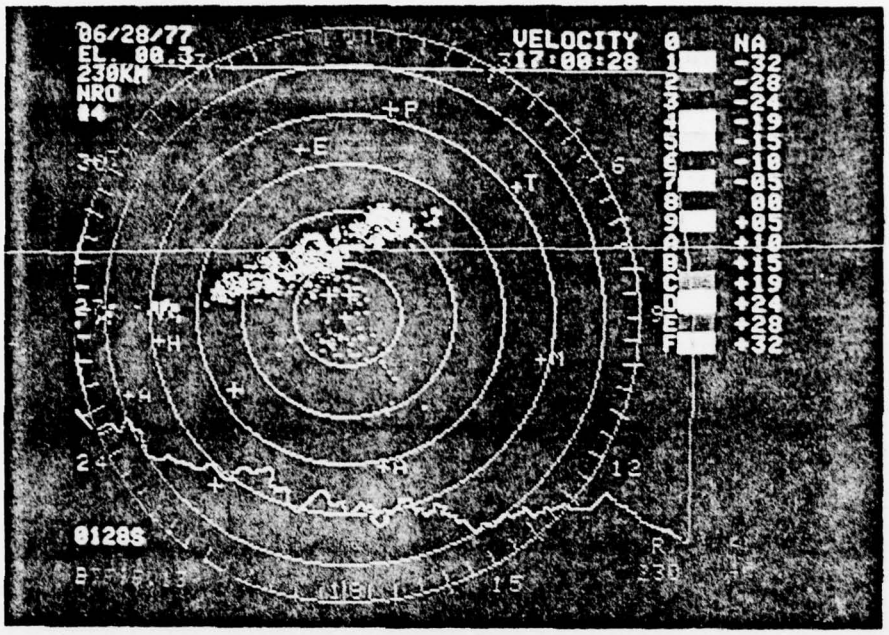

(b)

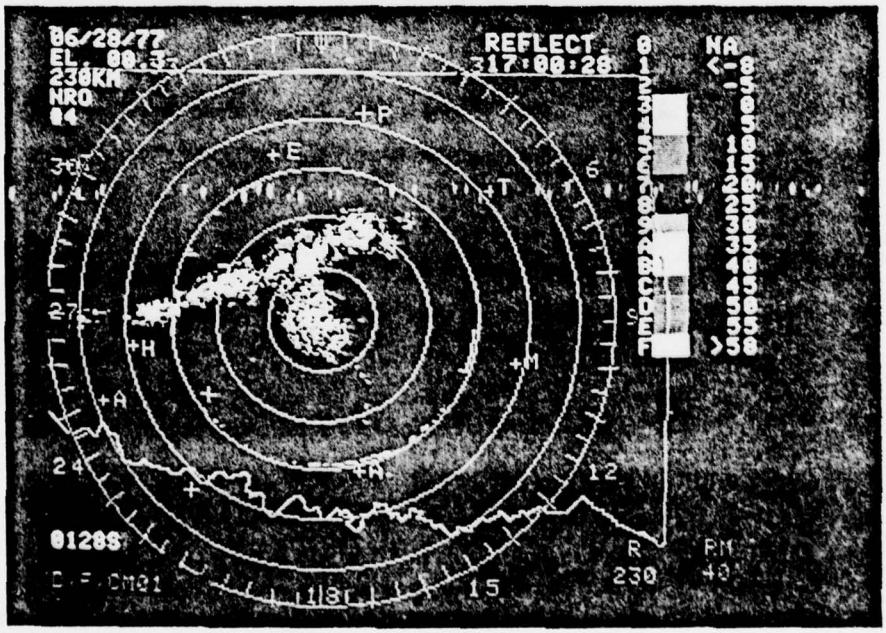

Figure A-5. Same as Figure A-4, but at 1700 CST.